PB84-232545

Spatial and Temporal Interpolation of Neros Radiosonde Winds

(U.S.) Environmental Sciences Research Lab.
Research Triangle Park, NC

Aug 84

U.S. Department of Commerce
National Technical Information Service
NTIS

PB84-232545

EPA-600/3-84-086
August 1984

SPATIAL AND TEMPORAL INTERPOLATION OF NEROS RADIOSONDE WINDS

by

O. Russell Bullock, Jr.
Meteorology and Assessment Division
Environmental Sciences Research Laboratory
Environmental Protection Agency
Research Triangle Park, North Carolina 27711

Project Officer

Francis S. Binkowski
Meteorology and Assessment Division
Environmental Sciences Research Laboratory
Environmental Protection Agency
Research Triangle Park, North Carolina 27711

ENVIRONMENTAL SCIENCES RESEARCH LABORATORY
OFFICE OF RESEARCH AND DEVELOPMENT
ENVIRONMENTAL PROTECTION AGENCY
RESEARCH TRIANGLE PARK, NORTH CAROLINA 27711

REPRODUCED BY
NATIONAL TECHNICAL
INFORMATION SERVICE
U.S. DEPARTMENT OF COMMERCE
SPRINGFIELD, VA. 22161

TECHNICAL REPORT DATA
(Please read Instructions on the reverse before completing)

1. REPORT NO.	2.	3. RECIPIENT'S ACCESSION NO.
EPA-600/3-84-086		PB84 232545

4. TITLE AND SUBTITLE	5. REPORT DATE
SPATIAL AND TEMPORAL INTERPOLATION OF NEROS RADIOSONDE WINDS	August 1984
	6. PERFORMING ORGANIZATION CODE
7. AUTHOR(S)	8. PERFORMING ORGANIZATION REPORT NO.
O. Russell Bullock, Jr.	
9. PERFORMING ORGANIZATION NAME AND ADDRESS	10. PROGRAM ELEMENT NO.
(same as box 12)	CDWA1A/02-2389 (FY84)
	11. CONTRACT/GRANT NO.
12. SPONSORING AGENCY NAME AND ADDRESS	13. TYPE OF REPORT AND PERIOD COVERED
Environmental Sciences Research Laboratory--RTP, NC Office of Research and Development U. S. Environmental Protection Agency Research Triangle Park, NC 27711	Final
	14. SPONSORING AGENCY CODE
	EPA/600/09

15. SUPPLEMENTARY NOTES

16. ABSTRACT

This research program was initiated with the overall objective of determining a most appropriate numerical method for the spatial and temporal analysis of free atmospheric, radiosonde derived, wind observations for the NEROS pollutant transport model. The analysis was to be performed by automated data processing under certain restrictions in computation time and storage area.

Previously developed methods of spatial and temporal data analysis were reviewed and their applicability to the NEROS effort were evaluated. Evaluation was based on tests with actual radiosonde data and with data sets produced through numerical model initialization procedures. In all cases, the desired result was a 7 by 6 grid of wind vectors in latitude-longitude space, for every hour during a three day test period.

Optimization of applicable spatial analysis schemes was completed and error statistics were calculated based on agreement between analysed grids and observed or computed data at various locations within the NEROS test region. Linear and curvilinear time interpolation methods were tested by applying them to data points before the spatial analysis, and by applying them to grid point values produced by previous spatial analyses.

17. KEY WORDS AND DOCUMENT ANALYSIS

a. DESCRIPTORS	b. IDENTIFIERS/OPEN ENDED TERMS	c. COSATI Field/Group

18. DISTRIBUTION STATEMENT	19. SECURITY CLASS *(This Report)*	21. NO. OF PAGES
RELEASE TO PUBLIC	UNCLASSIFIED	93
	20. SECURITY CLASS *(This page)*	22. PRICE
	UNCLASSIFIED	

EPA Form 2220-1 (9-73)

NOTICE

This document has been reviewed in accordance with U.S. Environmental Protection Agency policy and approved for publication. Mention of trade names or commercial products does not constitute endorsement or recommendation for use.

AFFILIATION

Both the author and project officer are on assignment from the National Oceanic and Atmospheric Administration, U.S. Department of Commerce.

ABSTRACT

The overall objective of this research program was to determine the most appropriate numerical method for the spatial and temporal analysis of free atmospheric, radiosonde-derived wind observations for the Northeast Regional Oxidant Study (NEROS) pollutant transport model. The program included analysis by automated data processing, under certain restrictions in computation time and storage area.

Previously developed methods of spatial and temporal data analysis were reviewed and their applicability to the NEROS effort was evaluated. This evaluation was based on tests with radiosonde data that had been collected from 24 locations in eastern North America and Bermuda and on artificial data sets that were produced for those locations through numerical model initialization procedures.

Three types of spatial wind analysis methods were investigated. Type 1 used wind component decomposition into two orthogonal horizontal directions. Type 2 used a separate analysis of wind speed in conjunction with directional guidance as obtained from a Type 1 analysis. Type 3 used vorticity and divergence guidance to define the wind field through the Helmholtz relation. In all cases, the desired product was a 7 by 6 grid of wind vectors in longitude-latitude space, centered over the NEROS model region.

Optimization of each of the three types of spatial analysis methods was performed. The greatest accuracy resulted from a Type 1 procedure, using simple directional wind components. The optimum Type 2 procedure was comparable in accuracy to the Type 1, and the more complex Type 3 procedure was shown to be the least accurate because of greater smoothing in the resultant analysis.

The investigation into temporal analysis dealt with the linear and curvilinear interpolation of radiosonde data and previously produced grid point winds, both available every 12 hours. The desired final product was spatial grids of wind vectors for every hour. Spatial and temporal analysis could not be performed simultaneously. Such an analysis using time as a third dimension was not undertaken because of the complications involved in mixing time and length scales. The spatial analysis was performed first, followed by the time interpolation of individual grid point values to most accurately produce intermediate wind fields in time.

This investigation was conducted under the sponsorship of the U.S. Environmental Protection Agency, Research Triangle Park, North Carolina, in conjunction with thesis preparation for a Masters of Science Degree in Meteorology at North Carolina State University.

CONTENTS

Abstract iii
Figures vi
Tables vii
Acknowledgments viii

1. Introduction 1
2. Conclusions and Recommendations 3
3. Materials and Methods
   - Data resources and test environment 5
   - Computer resources and the computational grid 7
4. Experimental Procedures
   - Two-dimensional gridding schemes for scalar variables . . 11
   - Wind analysis by component decomposition 19
   - Wind definition and analysis based on vorticity and divergence 27
   - Sensitivity testing and optimization of the adopted process 36
5. Results and Discussion
   - Temporal Interpolation for NEROS 40
   - User guide to NEROS wind analysis software 43

References 45
Appendices

A. Surface and 700 mbar charts 47
B. Artificial fields of 700 mbar height and gradient wind 62
C. Examples of preliminary, measured, and final analysis fields from the Schaefer-Doswell procedure 69
D. Calculation of gradients from the method of overlapping polynomials 74
E. Error fields on 9 by 5 test matrix using the Schaefer-Doswell procedure on actual data 76
F. Error fields on 9 by 5 test matrix using the Schaefer-Doswell procedure on artificial data when a modified Barnes routine is used to grid measured values of vorticity and divegence . . 78
G. Error fields on 9 by 5 test matrix using the Schaefer-Doswell procedure on artificial data when a pure Barnes routine is used to grid measured values of vorticity and divergence . . . 82

FIGURES

Number		Page
1	Map of the test region with the locations of all available radiosonde stations denoted by stars	6
2	Example of an "overlapping polynomial" fit to four points . .	8
3	Example of a two-dimensional interpolation using the method of "overlapping polynomials"	8
4	Computational grid superimposed on a regional map showing the outline of the wind analysis test region	10
5	Example of the conservation of gradient problem	13
6	Example of the "one over r squared" method of analysis . . .	15
7	Example of the pure Barnes method of analysis	17
8	Example of the tangent plane method of analysis	18
9	Example of the hybrid method of analysis	20
10	Example of wind interpolation non-uniqueness	21
11	Example of deformation wind field analysis	27

TABLES

Number		Page
1	Error Evaluation for Six-way Test of Wind Gridding Schemes and Decomposition Types - Actual Data	23
2	Error Evaluation for Six-way Test of Wind Gridding Schemes and Decomposition Types - Artificial Data	23
3	Error Evaluation for Optimization of Scheme Two Using "u,v" Wind Decomposition	25
4	Error Evaluation for Optimization of Scheme Two Using "u,v,s" Wind Decomposition	26
5	Error Results for the Adopted Wind Analysis Process	39
6	Error Results for Time Interpolation Procedure One	41
7	Error Results for Time Interpolation Procedure Two	41

ACKNOWLEDGEMENTS

The cooperation of the Environmental Sciences Research Laboratory personnel in general is greatfully acknowledged. I would like to express my sincere gratitude to Dr. Francis S. Binkowski for his instruction and guidance throughout the course of this research effort. His membership on my graduate research committee at North Carolina State University, during this combined academic and professional research effort, was a considerable asset to me. Special thanks is also given to another individual, James M. Godowitch, for his technical review of this report.

SECTION 1

INTRODUCTION

The purpose of this research is to investigate the process of spatial interpolation and analysis of free atmospheric winds through weighted averaging of directional components and through more sophisticated processes involving the analysis of vorticity and divergence.

Spatial wind analysis mostly pertains to the estimation of winds at predefined, rectangularly spaced grid points lying on a particular horizontal plane. These rectangular grids are often used to calculate prognostic meteorological models or to determine the transport quantities of pollutants in dispersion models. For this research, the latter use is assumed.

The measurement of wind at heights of more than 1000 meters above the ground is usually performed by releasing helium filled balloons having a rate of ascent on the order of 10 m/s, tracking the balloons by using optical or radar equipment, and recording the horizontal component of their motion as they ascend. These meteorological balloons often carry a radio transmitting package that relays the temperature, pressure, and humidity measured by onboard sensors during the flight. The radio sounding packages are sometimes lifted to heights exceeding 20 km before the reduced ambient pressure causes the balloon to expand beyond its capacity and burst. The package then descends on a small parachute that prevents a damaging impact on the earth's surface.

For most meteorological purposes, winds measured at various vertical levels are assumed to be valid over the release point, because of the rapid ascent of the balloon and the horizontal scale of the wind features that are predominant at higher levels. Wind measurements from radiosonde balloons are obtained for many vertical levels during each flight. For this study, a wind measurement is assumed to be available from each radiosonde flight at the vertical level of analysis. Thus, the analysis procedure entails a two-dimensional interpolation of wind values measured at scattered horizontal locations to the predefined horizontal grid points.

Wind is a vector that is often decomposed into directional components so it can be defined it in terms of scalars. These components are the eastward component, "u", and the northward component, "v", of the wind vector pointing in the direction of air flow. Many types of two-dimensional analysis schemes exist for scalars, vectors, or both. Because the spatial analysis of scalars is more straightforward, the wind

components are often analyzed separately and recomposed to get a wind field estimate. The problems with this analysis method have been noted and qualitatively studied. The applicability of this method seems to depend greatly on certain characteristics of the wind flow pattern being analysed.

This research effort is designed to measure the accuracy with which wind decomposition into "u,v" components can be used for the spatial analysis of free atmospheric winds by weighted averaging, and to investigate more sophisticated wind field analysis methods that recognize wind as a vector quantity. Therefore, analyses based on actual and artificial radiosonde data for the 700 millibar (mbar) pressure level were performed by various methods, and their accuracy was evaluated at data locations and at regularly spaced locations throughout the analysis region.

SECTION 2

CONCLUSION AND RECOMMENDATIONS

The results from the wind analysis by component decomposition suggest that analysis of 700 mbar wind into only its directional components (u,v) yields about the same accuracy as when the wind direction is determined from the "u,v" decomposition and the speed is determined by a separate analysis of observed wind speeds. However, different results may be obtained if a more complex wind pattern is analyzed, because the deviation of numerically analyzed winds from those analyzed manually appears to depend on convergent deformation in the wind field.

The scalar gridding scheme that most accurately reproduced the artificial wind field was similar to that defined by Barnes (1973) except that only the closest 30% of the available grid points is used to produce each grid point estimate. This stipulation seems to enable the scheme to respond to varying data density from one portion of the analysis region to another. Derivation of an analytical wave response function for this scheme, based on the methods used by Barnes (1973), was not possible because of the complicating effect of a finite scanning distance on the fundamental equations Barnes used to derive his wave response function.

One possible problem of this modified gridding scheme involves the wave scale mixing that occurs as part of the adjustment to data density. Use of this scheme to provide initial conditions for a prognostic numerical model may be detrimental. However, this scheme is the most accurate method for the determination of transport winds for use in pollution dispersion models.

The analysis of wind based on vorticity and divergence analysis, as proposed by Schaefer and Doswell (1979), results in greater average errors than analysis by simple "u,v" decomposition. The sensitivity testing of this method determined that the optimum procedure resulted in root mean square (RMS) errors of about 1.6 m/s, while the optimum "u,v" decomposition method produced errors of about 1.0 m/s. However, this difference of 0.6 m/s is rather insignificant when the accuracy of standard radiosonde observations in the middle troposphere is considered. Investigation by Kurihara (1961) of errors in radiosonde observations suggested a standard deviation of over 2 m/s at the 700 mbar level.

The main fault of the Schaefer-Doswell scheme as implimented for this study, is the computing time required to estimate the triangle centroid estimates of vorticity and divergence and to grid these

estimates for use as the forcing functions for the wind field. Execution times for the procedure vary between 5 and 40 s, depending on the triangle criteria specified. For example, the most accurate Schaefer-Doswell procedure required about 9 s, while the best "u,v" decomposition method required about 1 s. Further refinement of the software used to perform the more complicated wind analysis may eventually increase its efficiency, but additional effort will always be required for wind analysis based on vorticity and divergence analyses.

In conclusion, there is a possible application of the Schaefer-Doswell scheme, or any scheme based on wind analysis in terms of vorticity and divergence, which may prove invaluable to future investigators. This application involves the ability to adjust the measured divergence field at every vertical level in a three-dimensional model, thus allowing it to account for the attenuation that occurs with height in terrain induced vertical velocity. A careful adjustment to the divergence fields from those defined by the radiosonde observations might make it possible to account for terrain effects that are not resolvable from radiosonde wind data but have been detected from surface wind data and topographic information. Development of such a technique probably would require considerable investigation beyond the scope of this study, but the prospects of such an endeavor may warrant future investigation.

SECTION 3

MATERIALS AND METHODS

DATA RESOURCES AND TEST ENVIRONMENT

The test region consisted of the northeastern United States and a portion of southeastern Canada (Figure 1). More specifically, the region extended from 69 to 84 degrees west-longitude and 38 to 45 degrees north-latitude. In and around that region are 24 American and Canadian radiosonde launching stations that regularly report on conditions aloft every 12 H. These reports come at 0000 and 1200 Greenwich Mean Time (GMT) and are used by many public and private agencies.

An important aspect of these test data is the radiosonde observation void over the Atlantic Ocean. This lack of data is an unfortunate problem that meteorologists commonly encounter during their analysis of radiosonde data. Difficulties associated with the non-uniform scattering of observations vary according to the particular spatial analysis scheme being used. Because this condition occurs frequently, it should be included in the test environment of this study. Observations reported by the 24 stations between 0000 GMT, August 3, 1979, and 0000 GMT, August 6, 1979, are used as test input to various analysis schemes.

During this period, the passage of a complete synoptic scale wave and several short wave features occurred at the 700 mbar level. As shown by surface and 700 mbar charts in Appendix A, these waves were associated with a cold front at the surface, which moved out of Canada and advanced south to the Carolinas and east into the Atlantic Ocean, spawning a squall line as it passed offshore in the New York City area. The passage of such a well-defined wave feature, with its attending fields of vorticity, divergence, and deformation, supplies a good sample of all common configurations of these fields.

The major shortcoming of this data set which was obtained from actual radiosonde observations, is the lack of data at the grid point locations for which the wind estimates are made. Therefore, to allow the establishment of a reference data value at any position on the test region, a data set was produced using analytical equations. A pressure surface height field was defined from two-dimensional trigonometric functions as demonstrated by Fritsch, Magaziner, and Chappell (1980), and the x-coordinate phase of the wave was iteratively shifted by one-sixth of its length to simulate the full eastward passage of a complex wave in the pressure pattern through six artificial data times.

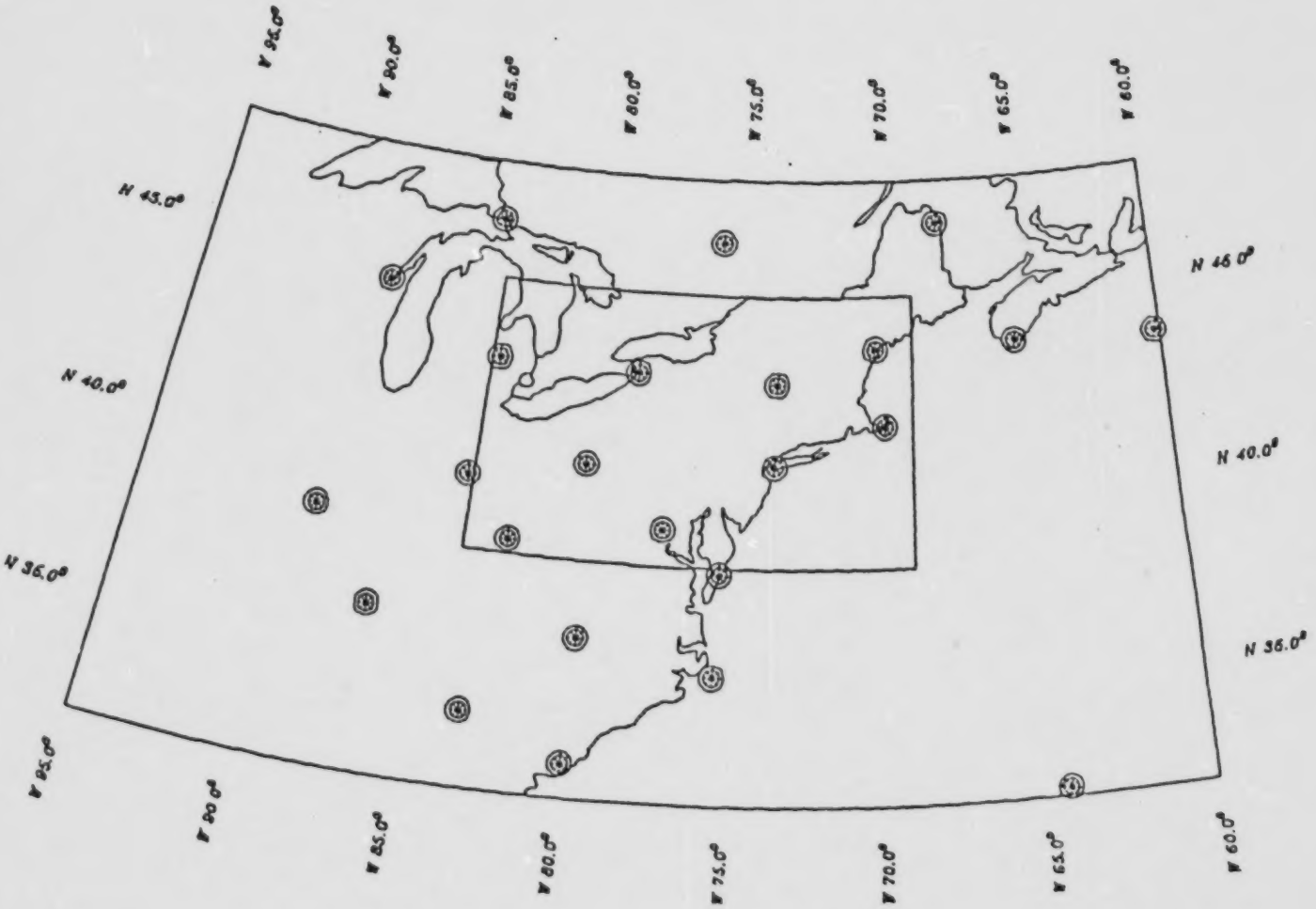

Figure 1 - Map of the test region with the location of all availible radiosonde stations denoted by stars.

Next, the gradient wind assumption was used to estimate the wind field associated with each of the six pressure surface height fields. These wind estimates were calculated for predefined test grid points. The establishment of this computational grid is discussed later in this section. The six 700 millibar height and gradient wind fields obtained by this process are displayed in Appendix B. Finally, to obtain gradient wind estimates for the radiosonde station locations, the method of overlapping polynomials was used to fit a surface to the gradient wind values obtained in the previous step. That surface was evaluated at the station coordinates to produce the sets of artificial data.

The method of overlapping polynomials used in this study is described by Bleck and Haagenson (1968). By this method, the two-dimensional interpolation is subdivided into many one-dimensional interpolations in the x and y directions. Each one-dimensional interpolation is achieved by using the four data points adjacent to the position of the estimate (Figure 2). Parabolic equations are determined for the data point sets (A,B,C) and (B,C,D). These parabolic functions are combined with a linear weighting function between the two central points of the parabolas. The process of extending this idea to two dimensions is illustrated in Figure 3.

For a true overlapping polynomial estimate in two dimensions, the interpolation position must be surrounded by 16 data points; however, for boundary cases, the single parabolic equation for the edge grid increment can be used for interpolation in either dimension. First, the one-dimensional interpolation scheme is used to estimate interpolated values at points A, B, C, and D, which have the y position of the desired interpolation location. Then, the values obtained for points A, B, C, and D, are used for an interpolation in the remaining dimension. Bleck and Haagenson determined that the particular dimension chosen for the first step interpolations has no effect on the final two-dimensional results.

These analytically produced data, which resemble the phenomena found in the real atmosphere, allow a stronger test of the analysis schemes surveyed in this study. Not only are the schemes tested for their ability to reproduce the observed winds at the observation point, but they are tested for their ability to interpolate and extrapolate the wind patterns to locations whose true wind conditions would otherwise be unknown.

COMPUTER RESOURCES AND THE COMPUTATIONAL GRID

All computer testing for this study was performed on the UNIVAC 1183 at the National Computing Center, Research Triangle Park, North Carolina. Account funding was provided by the U.S. Environmental Protection Agency (EPA) Meteorology Laboratory. All software for the spatial analysis of wind and graphic display of results using Tektronix Plot 10 and Hewlett-Packard HP-Plot/21 graphing packages was developed by the author using

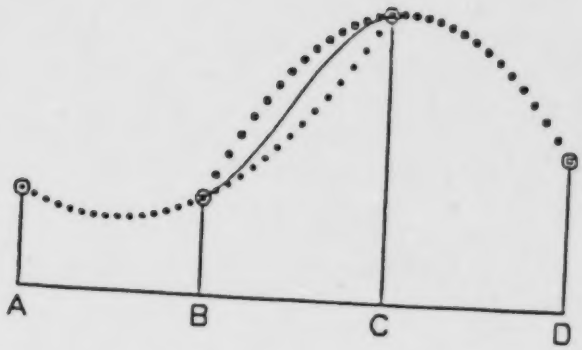

Figure 2 - Example of an "overlapping polynomial" fit to four points

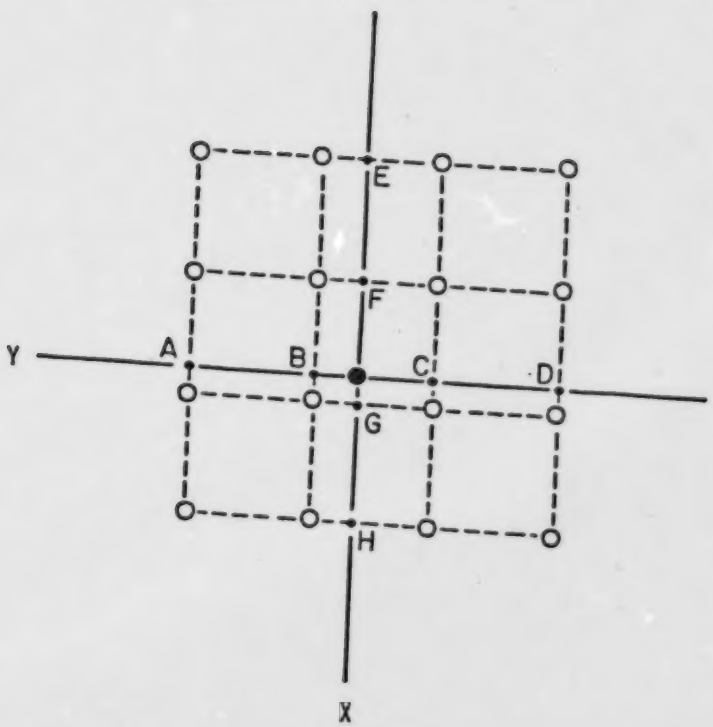

Figure 3 - Example of a two-dimensional interpolation using the method of "overlapping polynomials"

ASCII FORTRAN as the programming language unless otherwise noted. All graphic output was from the Hewlett-Packard 7221A table plotter or by hard copy from the Tektronix 4014-1 terminal.

The main storage requirements of any analysis package tested during this study should have been 64 K words or less because of requirements of economics and efficiency. Although the execution time for the various analysis schemes was not limited, it was examined and evaluated during the study. The establishment of the computational grid for testing the various analysis schemes was governed by both the computer storage limitations and the spatial density of the radiosonde reporting stations.

Like most synoptic scale meteorological computer models, the model grid for this study was defined on a spherical latitude-longitude surface. The vertical test level of 700 mbar was arbitrarily chosen to represent the free atmosphere. However, selection of the horizontal grid spacing was a more difficult task. A small grid point spacing is usually desired so that the smaller scales of the phenomena in question can be detected. However, halving the spacing of a two-dimensional grid results in four times the storage area and execution time requirements of the analysis scheme. Based on an estimated average radiosonde station spacing of km, and the knowledge that it would be unjustified to attempt to resolve those waves in the wind field that had lengths of less than twice the average station spacing, the grid spacing for this study was defined as one-fourth the wavelength of the smallest wave resolvable from the average radiosonde station spacing. This spacing of 200 km is approximated in latitude-longitude space near 42^0N by the grid spacing of 2^0 latitude and 3^0 longitude.

To center the grid over the previously defined test region and overlap it sufficiently to diminish any boundary problems, which often arise from numerical analysis, a 7 by 6 grid of longitude-latitude positions was chosen (Figure 4). The calculations of position and length-dependent quantities during this research were based on spherical geometry whenever feasible. The substitution of planar geometrical relations is noted throughout this text as part of the description of the analysis processes where they apply.

Figure 4 - Computational grid superimposed on a regional map showing the outline of the wind analysis test region

SECTION 4

EXPERIMENTAL PROCEDURES

TWO-DIMENSIONAL GRIDDING SCHEMES FOR SCALAR VARIABLES

Many approaches can be used to estimate grid point values when appropriate data points are available. Fourier analysis with periodic functions can be used; however, this approach leads to boundary problems and requires relatively large amounts of computer time. Least-squares surface fitting to data points is another approach that involves rather complex operations, which tend to exhaust computing resources. A simpler approach, which is commonly used is distance-based weighting of data points for the estimation of individual grid points. By this method, each grid point estimate is computed individually and less computer storage area is required during execution.

For distance-weighted analysis schemes, the ideal situation is for the grid point being estimated to be surrounded by randomly spaced data points on the plane of the analysis. Every data point, or a subset of data points, is examined for its value and distance from the grid point. If only subsets of the data points are scanned, the subset is usually based on a maximum distance from the grid point, or a maximum rank of proximity. In each case, the data point's value is multiplied by a weighting factor which is a function of the distance between the grid point and the data point. These distance-weighted contributions and their associated weighting factors are calculated and summed for all the data points being scanned. These operations are described by Equations 1 and 2. After data scanning is complete, the grid point estimate is obtained by dividing the sum of contributions by the sum of weighting factors, as in Equation 3.

$$\sum_{n=1}^{N} z_n w_n = \text{sum of contributions}, \quad N = \text{number of data points} \qquad (1)$$

$$\sum_{n=1}^{N} w_n = \text{sum of weights} \qquad (2)$$

$$f(i,j) = \sum_{n=1}^{N} z_n w_n \Big/ \sum_{n=1}^{N} w_n \qquad (3)$$

The most distinguishing characteristic of all distance-weighted analysis schemes is the function that defines the weighting factor. This function effects the resolution properties of the analysis, the sensitivity of the scheme to data point spatial distribution, and the computer execution time required to complete the analysis. While some schemes have additional iterative processes that enhance the final analysis, the basic performance characteristics of the scheme depend on the form of the weighting function.

One of the simplest forms for the weighting function is used by a type of scheme described as "one over R squared," the basic formula of its weighting function. While this description may not precisely define the weighting function, these weighting functions do take the form of a distance to a power, dividing a constant, as in Equation 4.

$$w_n = C/(r_n)^p \qquad r_n = [(x(i,j)-x_n)^2 + (y(i,j)-y_n)^2]^{1/2} \qquad (4)$$

However, this simplest and fastest method of analysis also tends to be the least rewarding. This scheme has two potential problems whose consequences depend on the circumstances of the analysis. One problem is the occurrence of singularities in the analysis attributed to the fact that as the separation distance between the grid point and the data point approach zero, the weighting function approaches positive infinity, resulting in the grid point estimate being exactly equal to the coincident data point, provided the numerical overflow point of the computer is not exceeded by the sum of the weighted data contributions. For some applications, this total acceptance of the single data point as truth is not a problem. But, the estimates for the grid points adjacent to this particular grid point will rapidly become more dependent on the average value of the surrounding data points as the separation from the previously coincident data point increases from zero; thus, singularity results.

The other problem with the "one over R squared" family of analysis schemes is usually less serious than the first. This problem pertains to the lack of conservation of gradient in the final analysis beyond the region of data points. As previously stated, the ideal condition is for the grid point to be surrounded by randomly scattered data, but this situation does not always exist. Distance-based weighting schemes generally do poorly when they are used for extrapolation, rather than the interpolation for which most were designed.

To examine this problem in two dimensions, picture a true line with a continuous slope down to the right (Figure 5, case A, B, and C). Assuming that measurements were reasonably accurate, data values would resemble the small stars shown in the figure. If an estimate were desired at the position of the dashed line in case A, then distance-weighted gridding would yield a good estimate. The contributed value from each data point is shown, and the weight given to it would be some inverse function of the distance. A crude representation of the resulting esti-

Figure 5 - Example of the conservation of gradient problem

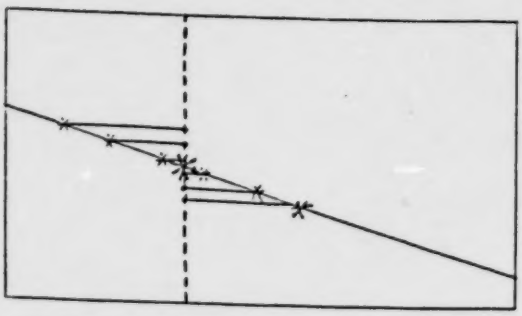

Case A - Conservation of gradient is not a problem for distance-weighted analysis schemes when an estimate (large star) is desired within a region of data points (small stars).

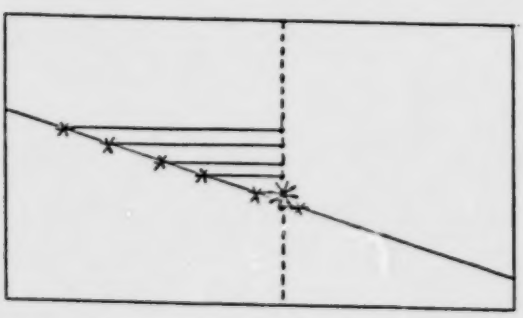

Case B - Distance-weighted analysis schemes may produce acceptable estimates near the boundary of data dense regions.

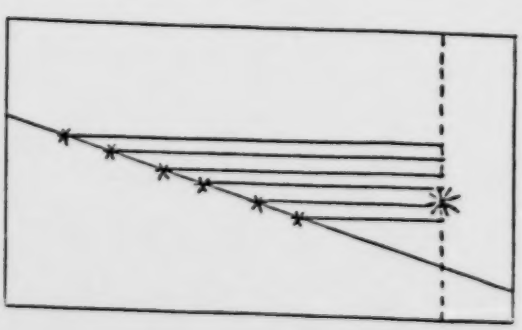

Case C - All distance-weighted analysis schemes produce poor results when forced to provide estimates outside the data region.

mate is given by the large star. A good estimate is also possible for case B. But, the estimate for case C is poor because of the influences of the distant data points and the lack of dependence on the predominant slope of the line. The result of such estimations in regions of sparse data is a fictitious wave in the analysis. When the "one over R squared" analysis method was used with test data, as shown in Figure 6, it resulted in an analysis that contained short wave features which were not justifiable given the average radiosonde station spacing.

Another type of distance weighting schemes commonly used is the "negative exponential" method, extensively studied by Barnes (1964, 1973). In this method, the weighting factor for each data point is a function of the exponent to the negative of the distance (r_n) (see Equation 5).

$$w_n = \exp(-r_n) \quad (5)$$

This scheme does not have the singularity problem at grid points that coincide with data points. As the separation distance approaches zero, the weighting factor approaches one, and arbitrary singularities are eliminated. Nevertheless, with this scheme, false waves are produced at data density discontinuities.

An investigation of the filtering properties of this scheme was conducted by Barnes (1964), during which he studied the conservation of waves of various lengths in the final analysis when the distance-based weighting function was given as,

$$w_n = \exp(-r^2/4C) \quad (6)$$

where "C" is a user defined scaling parameter.

Using Barnes' scheme, the scale of waves that are conserved in the final analysis can be varied. In addition, Barnes showed that the amplitude of all waves in the analysis will be somewhat diminished, but can be restored by noting the deviations of the analysis from the data, using the deviation values as data for a separate grid generation from the same weighting function, and subtracting the deviation grid from the first grid. This corrective procedure can be repeated numerous times for further restoration of desired wave features.

Later study by Barnes (1973) showed that the amplitude can be more completely restored and that the final filtering efficiency as a function of wavelength can be determined analytically. By using a smaller scaling parameter "C" in the corrective gridding procedure, the resulting larger adjustment to the preliminary analysis enables faster convergence toward the desired pattern resolution. However, the smaller scaling parameter used in the corrective pass reintroduces the existence of small scale

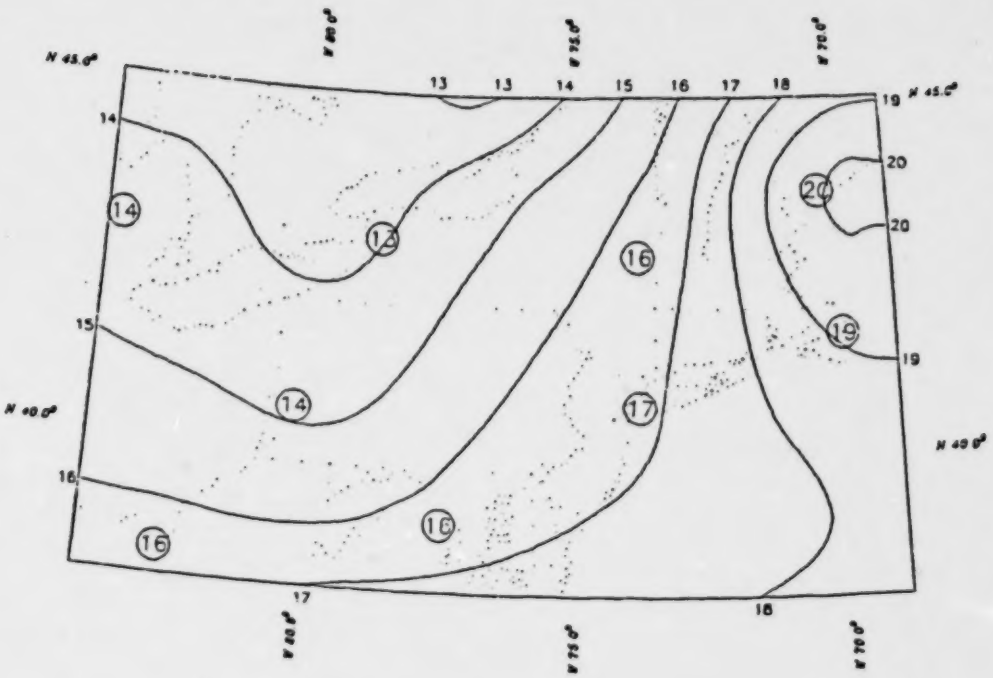

Figure 6 - Example of the "one over r squared" method of analysis (input data are denoted by circled numbers)

waves in the final analysis, that were filtered by the preliminary analysis, therefore, the minumum conserved wavelength in the final analysis is affected greatly by the value of the corrective scaling parameter. The corrective scaling parameter "CG" is defined as,

$$CG = G \times C, \qquad 0 < G < 1 \tag{7}$$

where smaller values of G allow the fastest convergence to the desired pattern resolution and smallest resultant wavelength features in the final analysis. Barnes showed that the proportion of the original wave that will be conserved (i.e., wave response) can be expressed by the following equation.

$$R = R_o(1 + R_o^{G-1} - R_o^{G}) \tag{8}$$

where R_o is the wave response from the preliminary grid generation, which is defined by the following equation.

$$R_o = \exp(-4C\pi^2/\lambda^2) \tag{9}$$

This scalar analysis scheme is not as simple and inexpensive to execute on a computer as the "one over R squared" method, but the problem of singularities in the analysis is solved, and the generation of false waves at data density discontinuities can be minimized because of the adjustable scaling parameters in the weighting function. A test example of this scheme, using data identical to that used with the "one over R squared" scheme, is shown in Figure 7.

In an attempt to conserve the gradients that are predominant in the data near the density discontinuity, an analysis procedure based on tangent plane estimations was tested. In this procedure, a tangent plane intersecting each data point is estimated using a least squares fit to surrounding data points. For the grid point estimate, each tangent plane for each data point, or a subset thereof, is extrapolated to the position of the grid point, and the resultant value is multiplied by a distance-based weighting factor. The result is a distance-based weighting scheme that measures not only the value of surrounding data points, but also the average slope of the data surface.

Figure 8 shows results from this "tangent plane" method when the closest half of the data points were used. The test data are the same as those used for previous examples. The increased gradient in the analysis at the lower right corner of the figure indicates that the gradient measurement worked. However, there is evidence of the same singularity problem found in the "one over R squared" method.

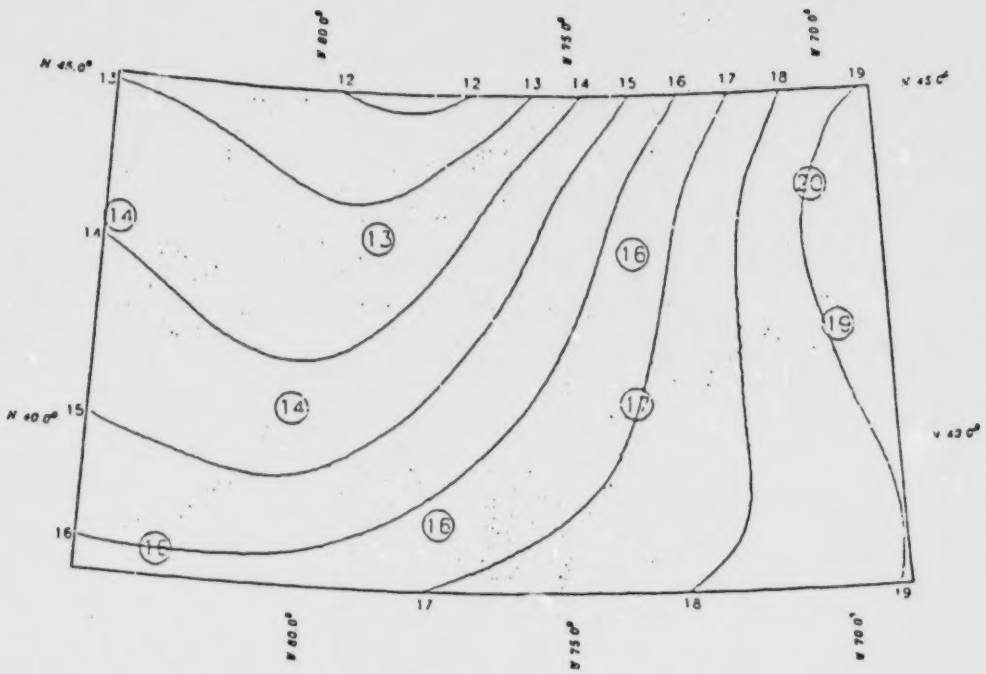

Figure 7 - Example of the pure Barnes method of analysis (input data are denoted by circled numbers)

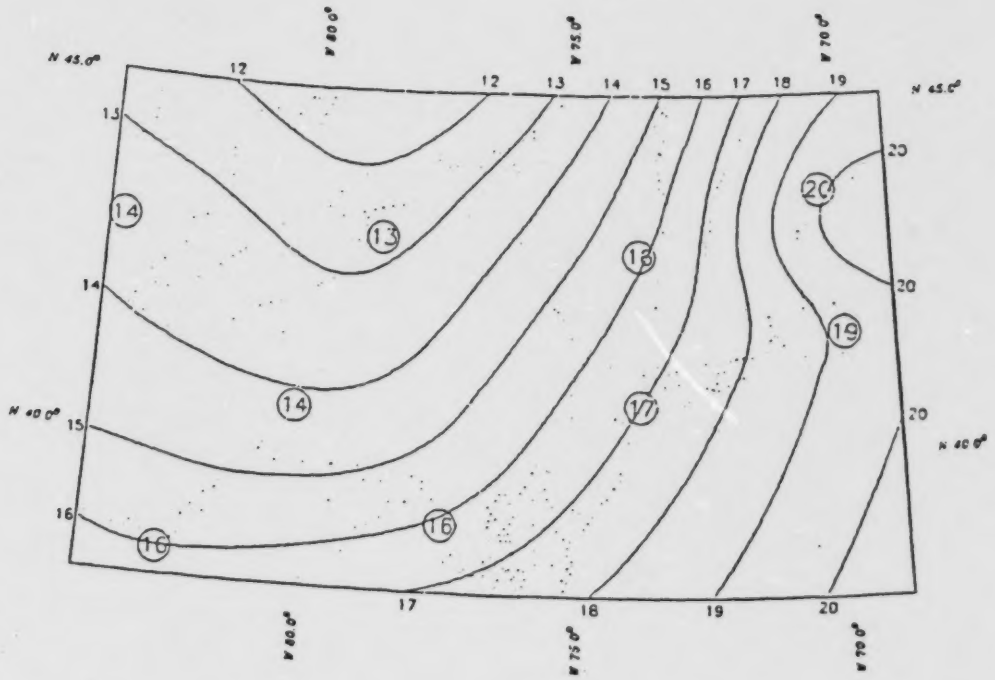

Figure 8 - Example of the Tangent Plane method of analysis (input data are denoted by circled numbers)

An important capability that is missing with this scheme is calculation of the wave response for different scales of waves. Experimentation indicates that as the number of data points and tangent planes used to make each estimate are increased, the smoothness of the analysis increases, but no specific function of wave response versus number of data points examined could be determined. Nor was a function available to express the effect of changes in the scaling parameter of the distance weighting function on the scale of wave conserved because of the random effects of tangent plane estimation and extrapolation.

To facilitate control over the scale of waves filtered by the analysis, a type of "hybrid" gridding scheme was developed. In this analysis procedure, the tangent plane projection method was used to produce a preliminary analysis that was designed to include all the wave features that could be substantiated by the spacing of the data points. These features were included by using only the five closest data points for the grid point estimate. Then, the preliminary grid of values was treated as data and a Barnes analysis was performed. The scaling parameters were chosen to filter waves that were shorter than twice the data spacing, thereby eliminating the unjustifiable wave features produced by the preliminary analysis. Figure 9 shows the results of this scheme when the test data of previous examples are used. As indicated, both the singularity and gradient conservation problems have been solved.

Testing of the analysis procedures discussed in this section, determined that the "one over R squared" and tangent plane extrapolation schemes produced analyses with sub-grid scale features associated with spatially coincident grid and data points, and thus were not suited for further investigation in the latter phases of this study. The Barnes and Hybrid schemes produced results that indicated their suitability for further study. However, all testing of analysis schemes previously discussed has been basically visual. The following text discusses the implementation of these schemes in actual wind analysis procedures and a more quantitative measure of their performance.

WIND ANALYSIS BY COMPONENT DECOMPOSITION

Numerical analysis of meteorological processes often involves the decomposition of wind vectors into two orthogonal scalar components. These components are "u", the easterly component, and "v", the northerly component of the wind vector pointing in the direction of wind flow. However, the ability of this decomposition to accurately reflect the true nature of fluid kinematics has been questioned. A lack of complete confidence in vector decomposition was expressed by Schaefer and Doswell (1979) when they stated;

"A fundamental problem in numerical analysis is that of non-uniqueness of vector field interpolation. This arises since a vector is a directed quantity. Interpolation of components does not necessarily yield the same results as interpolation of magnitude and direction. This

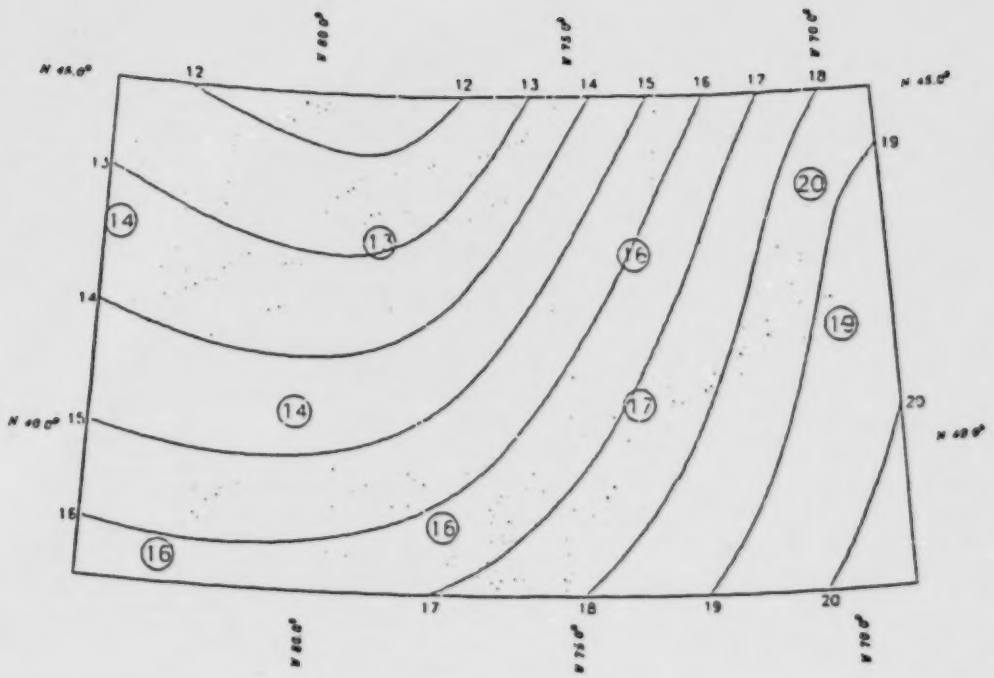

Figure 9 - Example of the Hybrid method of analysis (input data are denoted by circled numbers)

problem can have a significant impact on objective interpolation of the meteorological wind field."

As an example of non-uniqueness in vector interpolation, consider two wind observations illustrated in figure 10. The wind at A is from the west at 20 knots, and at C, the wind is from the south at 20 knots. Magnitude-direction interpolation to the midpoint B gives a wind of 20 knots from the southwest, while "u,v" component analysis gives a wind with components of 10 knots from the west and 10 knots from the south, resulting in a wind from the southwest as before, but with a speed of 14.14 knots. As the wind directions at the two data points become more opposite, the discrepancy between the two methods of interpolation increases. This difference indicates that in zones of convergent deformation, one of the two methods is not well suited for the analysis of wind.

In a study by Williams (1976), data that were interpolated by computer were compared to manually interpolated data. While the wind directions from each method usually agreed, the wind speeds differed by an average of 3.5 m/s.

Because the speed of the wind, not the direction, is where the discrepancy seems to occur most often, it has been suggested by a number of investigators that the direction of the wind field should be obtained by component analysis, and that the speed of the wind field should be analyzed independently. A promising aspect of this separate analysis of wind speed is that it allows a direct constraint to be applied to the resulting values of parcel acceleration from the wind analysis, and the average kinetic energy of the final wind analysis is based directly on measurements of kinetic energy. For this reason, the separate analysis of wind direction and speed was investiged during this study.

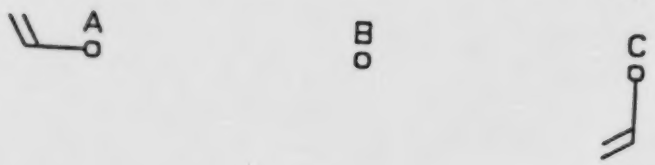

Figure 10 - Example of wind interpolation non-uniqueness

Tests on the regular wind component (u,v) method and on the separate speed analysis (u,v,s) method were conducted using both the data set derived from actual wind observations and the set of artificial data calculated from the gradient wind approximation and a pressure field defined from trignometric functions. For both methods, the separate components were analyzed using three different gridding schemes. Two of the gridding schemes were the Barnes type, and the other was a hybrid type, as discussed earlier in this section.

The Barnes schemes, 1 and 2, were different only in the definition of the subset of data points that were scanned for the estimation of each grid point. Scheme 1 scanned all data within 800 km of the grid point being estimated, while Scheme 2 scanned the closest half of the data points regardless of the distances involved. On the average, the closest half of the data points were within a radius of about 800 km. These schemes differ slightly from that suggested by Barnes (1964,1973); for reasons of economy and efficiency, only a subset (about half) of the data available were used to make grid point estimates. The other half had separation distances from the grid point of about one or more times the length of the predominant waves in the wind pattern. These points were believed to have little constructive effect on the distance-weighted estimations. Evidence to support this idea is discussed later in this section.

Scheme 3, the hybrid type, involved computing a preliminary grid using the five closest tangent planes and producing the final grid by applying Scheme 2 to the preliminary grid. This procedure is identical to that used to test the "hybrid" concept, which is discussed earlier in this section.

The two types of wind component analysis, each tested with three scalar analysis schemes, resulted in a six-way test. Error analysis was performed using the set of seven actual observations at the 700 mbar level. The root mean square and average absolute errors for each of the six tests are shown in Tables 1 and 2. Each error figure is derived from comparison of the analyzed wind at the reporting station locations to the observed wind at the stations. When seven separate analyses are performed, about 160 comparisons result for each test. Analyzed wind values for the station locations were obtained using the method of overlapping polynomials on the output wind grids, as described in Section 3.

The results show that the two Barnes schemes are nearly equal in most accurate cases, the (u,v,s) wind decomposition scheme seems to be slightly more accurate than the simple (u,v) scheme.

The test results from real data were obtained by comparison at station locations only; therefore, they do not represent a complete test. An analysis scheme such as the one based on two dimensional equation fitting may produce fields that match the data exactly, but this result proves nothing about the method's accuracy for interpolation or extrapolation. For this reason, the six-way test of wind decomposition and

Table 1 - ERROR EVALUATION FOR SIX-WAY TEST OF WIND GRIDDING SCHEMES AND DECOMPOSITION TYPES - ACTUAL DATA

Method	Station RMS error	Station AA error
Scheme 1 (u,v)	1.980 m/s	1.683 m/s
Scheme 1 (u,v,s)	1.956	1.672
Scheme 2 (u,v)	1.962	1.673
Scheme 2 (u,v,s)	1.939	1.655
Scheme 3 (u,v)	2.343	2.046
Scheme 3 (u,v,s)	2.415	2.116

Table 2 - ERROR EVALUATION FOR SIX-WAY TEST OF WIND GRIDDING SCHEMES AND DECOMPOSITION TYPES - ARTIFICIAL DATA

Method	Station RMS	Station AA	Grid point RMS	Grid point AA
Scheme 1 (u,v)	1.030 m/s	0.937 m/s	1.550 m/s	1.281 m/s
Scheme 1 (u,v,s)	1.030	0.919	1.559	1.285
Scheme 2 (u,v)	0.969	0.882	1.493	1.216
Scheme 2 (u,v,s)	0.973	0.870	1.503	1.226
Scheme 3 (u,v)	1.113	0.992	1.836	1.573
Scheme 3 (u,v,s)	1.153	1.015	1.871	1.596

RMS = root mean square error

AA = average absolute error

component gridding techniques also was conducted by using the set of artificial data that was prepared as discussed in Section 3. With this data set, the performance of the analysis procedure was tested at not only the station locations, but at every internal grid point. Results from this test, shown in Table 2, suggest that Scheme 2 is slightly superior to Scheme 1 and that Scheme 3 is a poor method to use for both the (u,v) and the (u,v,s) decomposition. Also, no evidence suggests that the (u,v,s) decomposition method is more accurate than the simple (u,v) method. However, the complexity of the wind pattern being analyzed may affect their relative accuracies.

The error quantities used in this study are not scaled to the data; therefore, comparisons of accuracy should not be made between tests with actual data and tests with artificial data. The average magnitude and variance of the two data sets are not necessarily equal, and tests conducted with the data set of greatest variance or complexity would likely result in the largest errors.

The only difference between Schemes 1 and 2 was the method used to chose the data points to be scanned; therefore, this must account for the difference in accuracy. Scheme 2 incorporates a dependence of the maximum data point to grid point separation on the data density near the grid point. Intuitively, if any contribution from distant data points is included in the estimation of a grid point, the randomness of the short wave components in the values of those distant data points will suppress the influence of the short waves on the grid point estimate because of the averaging of their random contributions. Therefore, decreasing the distance to which the data points are scanned should decrease the filtering of short waves. Scheme 2 scans to a shorter distance when data are more dense, and shorter waves in the analysis can be justified.

In an attempt to optimize Scheme 2, the scanned proportion of the data points was varied from one-tenth to ten-tenths, and the error analyses were performed as before. Tables 3 and 4 show that the results vary when different locations are used to calculate error. The test using actual data, where errors were obtainable only at the stations, indicates that the best performance is obtained when the fewest data points are scanned. The station location error analysis using the artificial data suggests the same conclusion. But, when errors are calculated throughout the analysis region, an optimum fraction of three-tenths is obtained.

This result reflects that when very few data points are scanned, the closest data point has a great influence on the estimate at the grid point. When all the estimates that make up the analysis are tested by comparison at only the station locations, mainly the grid point estimates near the stations are tested, and the average error, in this case, will be small. Therefore, the error analysis based on station location comparisons is not a valid test of a scheme's performance. For this reason, three-tenths is judged to be the best fraction of data points tc be scanned when working with the spatial data distribution and pattern resolution scale adopted for this study.

Table 3 - ERROR EVALUATION FOR OPTIMIZATION OF SCHEME TWO USING "u,v" WIND DECOMPOSITION

(All errors are in units of meters per second)

	ACTUAL DATA (stations)		ARTIFICIAL DATA (stations)		ARTIFICIAL DATA (grid points)	
Fraction	RMS	AA	RMS	AA	RMS	AA
0.1	1.157	.982	.611	.543	1.768	1.360
0.2	1.860	1.618	.848	.739	1.416	1.088
0.3	1.896	1.628	.803	.723	1.345	1.033
0.4	1.946	1.659	.921	.839	1.465	1.183
0.5	1.961	1.674	.969	.882	1.493	1.216
0.6	1.967	1.678	.987	.897	1.506	1.228
0.7	1.969	1.677	1.001	.913	1.520	1.245
0.8	1.970	1.677	1.004	.916	1.523	1.249
0.9	1.970	1.677	1.005	.917	1.524	1.250
1.0	1.970	1.677	1.005	.917	1.524	1.250

RMS = root mean square error

AA = average absolute error

Table 4 - ERROR EVALUATION FOR OPTIMIZATION OF SCHEME TWO USING "u,v,s" WIND DECOMPOSITION

(All errors are in units of meters per second)

	ACTUAL DATA (stations)		ARTIFICIAL DATA (stations)		ARTIFICIAL DATA (grid points)	
Fraction	RMS	AA	RMS	AA	RMS	AA
0.1	1.194	1.006	.612	.545	1.775	1.365
0.2	1.826	1.580	.851	.745	1.413	.084
0.3	1.861	1.602	.810	.722	1.352	1.04
0.4	1.922	1.638	.928	.831	1.473	1.193
0.5	1.939	1.656	.973	.870	1.503	1.226
0.6	1.943	1.661	.990	.884	1.516	1.237
0.7	1.945	1.660	1.004	.898	1.529	1.254
0.8	1.946	1.660	1.007	.901	1.532	1.257
0.9	1.946	1.660	1.008	.902	1.533	1.258
1.0	1.946	1.659	1.008	.902	1.533	1.258

RMS = root mean square error

AA = average absolute error

WIND DEFINITION AND ANALYSIS BASED ON VORTICITY AND DIVERGENCE

In this section, a process for the analysis of wind fields using vorticity and divergence is presented. Methods for obtaining and using these quantities to define the final wind analysis are included. The process adopted for this study is the one considered to be best suited for use, given the data and computing limitations previously discussed. Reasons for selection or non-selection of various operations toward the compilation of the process are explained, and sensitivity testing of the adopted process is discussed at the end of this section.

As previously stated, wind is a vector quantity with known behavioral characteristics. Vorticity and divergence each describe a particular vector field characteristic. Individual vectors can be fully expressed in terms of orthogonal components or components of direction and magnitude. Therefore, interpolation of vectors using scalar component analysis is a non-unique process, and the results obtained by one process may be different from the results obtained by another.

Vorticity and divergence are defined by spatial gradients of directional vector components and are not affected by rotations of the coordinate plane on which the components are based. These characteristics would seem to make vorticity and divergence the most universal measures of vector fields. For this reason, vector field analysis is often performed using constraints on vorticity and/or divergence.

An example of a weakness of wind interpolation using simple directional component analysis is illustrated in Figure 11. The convergent deformation line is a phenomenon common to frontal boundaries both at the surface and aloft. The results of component interpolation to the convergence line, shown in the left half of the figure, are contrary to what is characteristic of the atmosphere. Because deformation is a vector field description that is defined by a different combination of the same component gradients that define both divergence and vorticity, it is believed that analysis of divergence and vorticity will allow a better representation of deformation in the final wind analysis, as shown in the right side of Figure 11.

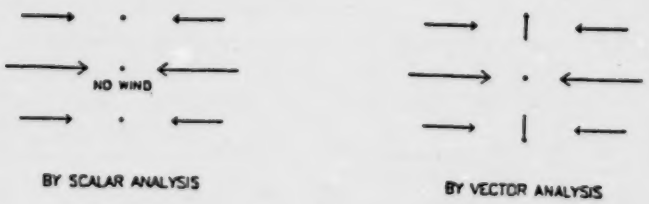

Figure 11 - Example of deformation wind field analysis

The structure of the horizontal wind field can be defined in terms of vorticity and divergence through use of the Helmholtz equation,

$$V = \vec{k} \times \nabla\Psi + \nabla\chi \tag{10}$$

separating the wind into its divergent and rotational components. Thus the cartesian components of the wind can be expressed as follows,

$$u = -\partial\Psi/\partial y + \partial\chi/\partial x \tag{11a}$$

$$v = \partial\Psi/\partial x + \partial\chi/\partial y \tag{11b}$$

where Ψ is often called the stream function, and χ, the velocity potential. The stream function has been used often in tropical weather analysis where wind-pressure relationships are more complex than those in the middle latitudes. A line of constant stream function value on an analysis should coincide with a streamline on the actual wind field. The velocity potential has been used with the stream function to better incorporate the effects of divergence into the final wind analysis. The values of the stream function and velocity potential are intimately dependent on the fields of vorticity and divergence, respectively. The stream function field is defined by the relation,

$$\nabla^2\Psi = \zeta \tag{12}$$

where ζ is vorticity, and the velocity potential field by the relation,

$$\nabla^2\chi = \delta \tag{13}$$

where δ is divergence. Equations 12 and 13 represent Dirichlet problems where the field of the forcing function can be determined and where the boundary values of the functions in question must be estimated.

The forcing fields of vorticity and divergence must be obtained from a preliminary wind field analysis or a direct evaluation of the parameters at discrete points in the analysis region. One of the first methods for direct evaluation of vorticity and divergence was proposed by Bellamy (1949). By assuming that the wind field varies linearly between observations, this method provides a point estimate of vorticity and divergence at the centroid of a triangle whose vertices are at wind observations. This method was based on the rate of change of the triangular area when the vertices follow the air parcels that were initially at the observation points.

With the advent of automatic data processing, Endlich and Clark (1963) introduced a procedure by which many dynamic variables can be determined. Divergence and vorticity are based on the linear wind variation assumption over the area of a triangle formed by observations. Thus, the wind at the centroid of the triangle is equal to the vector average of the three vertex wind observations as given below.

$$u_o = (u_1+u_2+u_3)/3 \tag{14a}$$

$$v_o = (v_1+v_2+v_3)/3 \tag{14b}$$

Then the wind at each vertex can be equated to a linear, two-dimensional Taylor series for each component, as in Equation 15.

$$u_i = u_o + (\partial u/\partial x)(x_i-x_o) + (\partial u/\partial y)(y_i-y_o) \tag{15a}$$

$$v_i = v_o + (\partial v/\partial x)(x_i-x_o) + (\partial v/\partial y)(y_i-y_o) \tag{15b}$$

where i = 1, 2, and 3. By subtracting the equation for vertex 1 from that for vertex 2, and from that for vertex 3, two simultaneous equations result for each component. Then these equations can be solved to obtain the component derivatives for the entire triangle. The simultaneous equations are as follows.

$$u_2 - u_1 = (x_2-x_1)(\partial u/\partial x) + (y_2-y_1)(\partial u/\partial y) \tag{16a}$$

$$u_3 - u_1 = (x_3-x_1)(\partial u/\partial x) + (y_3-y_1)(\partial u/\partial y) \tag{16b}$$

$$v_2 - v_1 = (x_2-x_1)(\partial v/\partial x) + (y_2-y_1)(\partial v/\partial y) \tag{16c}$$

$$v_3 - v_1 = (x_3-x_1)(\partial v/\partial x) + (y_3-y_1)(\partial v/\partial y) \tag{16d}$$

When solved for the wind component derivatives Equation 16 gives,

$$\partial u/\partial x = ((u_2-u_1) - \alpha_y(u_3-u_1)) \,/\, ((x_2-x_1) - \alpha_y(x_3-x_1)) \tag{17a}$$

$$\partial u/\partial y = ((u_2-u_1) - \alpha_x(u_3-u_1)) \,/\, ((y_2-y_1) - \alpha_x(y_3-y_1)) \tag{17b}$$

$$\partial v/\partial x = ((v_2-v_1) - \alpha_y(v_3-v_1)) \,/\, ((x_2-x_1) - \alpha_y(x_3-x_1)) \tag{17c}$$

$$\partial v/\partial y = ((v_2-v_1) - \alpha_x(v_3-v_1)) \,/\, ((y_2-y_1) - \alpha_x(y_3-y_1)) \tag{17d}$$

where $\alpha_x = (x_2-x_1) \,/\, (x_3-x_1)$ and $\alpha_y = (y_2-y_1) \,/\, (y_3-y_1)$.

By the linear variation of wind assumption, these first-order derivatives are applicable to the entire area of the triangle and are valid at the location of the centroid. The point estimates of vorticity and divergence can then be calculated for these centroids. Many possible triangle triplets exist within the network of the radiosonde stations for this study. Therefore, many wind derivative point estimates can be made to define the forcing fields of vorticity and divergence. An additional reward with this technique is the ability to make parameter estimates for locations over part of the Atlantic Ocean, because of the baylike curvature of the shoreline in the analysis region. In a more general sense, this technique will allow calculation of vorticity and divergence values in a region of missing data if data are available around the periphery.

Ceselski and Sapp (1975) suggested that the shapes of the triangles used to make these estimates have an effect on the relative confidence that should be placed in each estimate. Triangles that are excessively nonequilateral tend to produce erratic estimates for the spatial derivatives. If the triangular station configuration is elongated in the x-direction, the resulting derivative estimates in that direction may be deficient in magnitude because of the scale filtering effects of the large x-distance between the stations, while y-derivative estimates will have no such smoothing, resulting in unreliable estimates of both vorticity and divergence. An underestimation of the magnitudes of both vorticity and divergence will result if the triangle is too large, because the derivative estimates from this method are areal average estimates for the region within the station triangle.

To study these scale filtering problems, a data point scanning routine was developed to generate all possible triangular combinations of radiosonde stations from the data network, eliminate those that did not meet specified size and shape limitations, and calculate the spatial gradients of the "u" and "v" wind components for the qualified triangles. These limitations were specified as input parameters for the scanning routine in the form of a maximum triangle area and a maximum triangle vertex angle ratio. The vertex angle ratio was defined as the maximum vertex angle of the station triangle, over the minimum vertex angle. This provided a measure of control over the elongation of the triangle, but not necessarily in the form of a linear relation.

The number of triangles which were produced, meeting the size and shape criteria, was limited to 500 because of constraints in computer storage and execution time. When this triangle overflow condition was reached during the scanning and cataloging of triangle data, the scanning operation was halted, a warning message was written to a data file monitoring the analysis procedure, and gridding of existing triangle data was begun. The wind analysis procedure was completed for truncated triangle data sets, but the results were not used in later sensitivity studies, which are discussed later in the this section.

No minimum size restrictions were used because the final fields of vorticity and divergence were to be determined with the scale-filtered

gridding routines discussed previously. Therefore, small-scale perturbations of these parameters, which were produced by the smaller triangles were filtered out of the analysis, as were all other sources of small scale noise. The discussion at the end of this section indicates the results obtained from a matrix that has the size and shape constraints used for both actual and artificial data sets.

A more sophisticated method for the estimation of first derivatives of any atmospheric quantity was developed by Chien and Smith (1973) in which second derivatives are included in the Taylor's series. The linear wind variation assumption was abandoned for this method, making it more applicable near jet streams and fronts where linearity generally does not exist. With this method, six wind observations are required, where five of them form a rough pentagon around the sixth. The central station provides information that is comparable to that which was estimated for the centroid in the Endlich and Clark triangle method. The outer stations are used to provide the five simultaneous equations necessary for solving the five unknown derivatives in the second-order Taylor's series. The resulting system of equations for the "u" component is expressed as,

$$u_i = u_0 + \left(\frac{\partial u}{\partial x}\right)_0 (x_i - x_0) + \left(\frac{\partial u}{\partial y}\right)_0 (y_i - y_0) + \frac{1}{2!}\left[\left(\frac{\partial^2 u}{\partial x^2}\right)_0 (x_i - x_0)^2 + 2\left(\frac{\partial^2 u}{\partial x \partial y}\right)_0 (x_i - x_0)(y_i - y_0) + \left(\frac{\partial^2 u}{\partial y^2}\right)_0 (y_i - y_0)^2\right] \qquad i=1\text{-}5 \tag{18a}$$

and for the v component as,

$$v_i = v_0 + \left(\frac{\partial v}{\partial x}\right)_0 (x_i - x_0) + \left(\frac{\partial v}{\partial y}\right)_0 (y_i - y_0) + \frac{1}{2!}\left[\left(\frac{\partial^2 v}{\partial x^2}\right)_0 (x_i - x_0)^2 + 2\left(\frac{\partial^2 v}{\partial x \partial y}\right)_0 (x_i - x_0)(y_i - y_0) + \left(\frac{\partial^2 v}{\partial y^2}\right)_0 (y_i - y_0)^2\right] \qquad i=1\text{-}5 \tag{18b}$$

The primary disadvantage to this scheme is its requirement for five wind observations surrounding the central observation point. The radiosonde data network for this study, with its 24 reporting stations, is not suitable for this application, especially when there are missing reports. On the average, only about 15 sets of six stations could be defined from the network, and the size of the pentagonal region over which the derivatives are defined resulted in the inability to resolve short wave features. These problems, and the substantial amount of computing time required to solve the system of five equations, made the scheme undesirable for further study.

It was decided that for the definition of the forcing fields of vorticity and divergence, the Endlich and Clark triangle gradient estimation method was most suitable. It could produce many point estimates of vorticity and divergence which could then be gridded using an appropriate analysis scheme to produce the forcing fields necessary for a wind analysis based on the Helmholtz theorem. Previously discussed tests of spatial analysis schemes for scalar quantities showed that a Barnes scheme using a predetermined number of closest data points was most

accurate in reproducing a test data field. This method was chosen for the analysis of point estimates of vorticity and divergence from the Endlich and Clark method, but a test with the quicker "pure" Barnes routine was also performed as part of the sensitivity study of the final wind analysis procedure.

Once the forcing fields of vorticity and divergence have been found, the boundary values of the stream function (Ψ) and velocity potential (χ) must be estimated. The Helmholtz equation provides the numerical link between the wind field and the fields of Ψ and χ. By this relation it is possible to estimate the boundary values of Ψ and χ when the boundary values of wind are known. For wind determination, only the gradients of Ψ and χ are relevent; therefore, it is possible to start at any point on the grid boundary with any value of Ψ and χ. Once the starting value and position have been chosen, by working along the circumference of the grid, Ψ and χ can be determined by the relations shown in Equations 19 and 20.

$$N \cdot V = N \cdot (k \times \nabla \Psi + \nabla \chi) = -\partial \Psi / \partial s + \partial \chi / \partial n = V_n \tag{19}$$

$$S \cdot V = S \cdot (k \times \nabla \Psi + \nabla \chi) = \partial \Psi / \partial n + \partial \chi / \partial s = V_t \tag{20}$$

where,

N = unit vector normal to the boundary pointing outward
S = unit vector tangent to the boundary pointing counterclockwise
n = normal distance on the earth positive outward
s = tangent distance on the earth positive counterclockwise
V_n = outward normal component of the wind at the boundary
V_t = counterclockwise tangential component of the boundary wind

From equation 19,

$$\partial \Psi / \partial s = -V_n + \partial \chi / \partial n \tag{21}$$

and from equation 20,

$$\partial \chi / \partial s = V_t - \partial \Psi / \partial n \tag{22}$$

and V_n and V_t can be estimated by a preliminary analysis of the wind.

Inspection of these equations reveals that in order to set the boundary values for Ψ, some knowledge about the field of χ is required, and similarly, to set values for χ, some knowledge of the field of Ψ is required. This dilemma can be solved only by making certain assumptions about at least one of the two parameters. If the boundary values of Ψ

are set first, then an assumption about the normal derivative of χ at the boundary has to be made which results in an assumption about the contribution of the velocity potential to the areal average divergence. If the boundary values for χ are set first, then an assumption about the normal derivative of Ψ at the boundary is required resulting in an assumption about the contribution of the stream function to the areal average circulation.

From the line integration of Equation 21 using the natural boundary conditions for a closed line integral, the following equation results.

$$\int(\partial\Psi/\partial s)ds = 0 = \int(-V_n + \partial\chi/\partial n)ds \qquad (23)$$

Therefore, even though the point values of $\partial\chi/\partial n$ along the boundary are not known, the average value on the boundary is obtainable from the average normal wind. This average value is the only point estimate available and it has to be used with the boundary values of V_n to get $\partial\Psi/\partial s$ and set the boundary values of Ψ. The result is a Ψ boundary value estimate based on the observed V_n and the assumption that the velocity potential contributes the same amount to V_n at all points on the boundary. This is equivalent to defining the stream function in terms of V_n^* only, where V_n^* is a non-divergent wind estimate defined by Equation 24,

$$V_n^* = V_n - (1/S)\int V_n ds = V_n - D \qquad (24)$$

where D is the areal average divergence, and S is the total boundary length.

This reliance on non-divergent wind estimates to set the boundary values of Ψ leads to a particular analysis problem that was discussed by Hawkins and Rosenthal (1965). In their study, a surface cyclone with true streamlines spiralling inward was analyzed by the constant $\partial\chi/\partial n$ method. The resulting stream function analysis showed an open wave with lowest Ψ values to the south. The distortion was attributed to the fact that the true wind field at the analysis level was not non-divergent. Setting the boundary values of the stream function by using the non-divergent wind estimate along the boundary resulted in an overly strong stream function field. In this case, the contribution of the divergent wind component was totally neglected, and the result was a Ψ field that attempted to account for all of the wind.

A similar boundary value problem can be obtained by linear integration of Equation 22, resulting in the following equation.

$$\int(\partial\chi/\partial s)ds = 0 = \int(V_t - \partial\Psi/\partial n)ds \qquad (25)$$

This equation, when treated in a similar manner as Equation 23, results in the definition of the velocity potential in terms of V_t^* only, where V_t^* is an irrotational wind estimate defined by the equation,

$$V_t^* = V_t - (1/S)\int(V_t)ds = V_t - C \qquad (26)$$

where C is the areal average circulation.

Setting the boundary values of the potential function first by using the irrotational wind estimate along the boundary results in an unnaturally strong field of velocity potential. In this case, the contribution of the rotational wind is totally neglected and the resultant χ field attempts to account for all of the wind.

In a study by Sangster (1960), a less hazardous method of calculating χ first was proposed. The boundary values of χ were set to zero all around the grid, and the previously defined field of divergence was used as the forcing function to define the χ field in the normal fashion. Next, the resultant values of $\partial\chi/\partial n$ and the values for the wind at the boundary were used to define the tangential gradient of Ψ for the determination of its boundary values. Sangster showed that setting χ by this method, for the purpose of determining Ψ boundary values, resulted in a maximization of the portion of the total kinetic energy carried by Ψ and minimized the portion carried by χ. Since vorticity is normally greater in magnitude than divergence in the free atmosphere, this result was considered to be positive. However, this relation between vorticity and divergence is not a rule of nature. Relative field strengths of the two parameters vary considerably, and techniques to account for this fact have been demonstrated.

A more contemporary scheme for balancing the proportions of the total kinetic energy carried by Ψ and χ was demonstrated by Schaefer and Doswell (1979). Noting that the bias between divergent and vortical energies is not constant, they proposed a method by which an adjustment to a preliminary wind analysis produces a final wind field that has a measured divergence and vorticity content without a direct manipulation of Ψ or χ fields. The measured content refers to the field strengths of vorticity and divergence determined by a separate analysis of each. These fields have been calculated for the determination of Ψ and χ, but by this method, they can be used directly to produce a final wind field.

The Schaefer-Doswell scheme uses two Lagrange multipliers, λ_2 and λ_2, which satisfy the following conditions,

$$\nabla^2\lambda_1 = 2(\zeta - k\cdot\nabla\times V_0) \qquad \lambda_1 = 0 \text{ on the boundary} \qquad (27a)$$

$$\nabla^2\lambda_2 = 2(\delta - \nabla\cdot V_0) \qquad \lambda_2 = 0 \text{ on the boundary} \qquad (27b)$$

where ζ and δ are the measured vorticity and divergence and V_o is the wind vector from the preliminary analysis.

After the multipliers are computed from these relations by using a relaxation routine, they are used to define the final wind field from the following relation.

$$V = V_o + (\nabla\lambda_2 + \vec{k}\times\nabla\lambda_1)/2 \qquad (28)$$

This wind analysis scheme has been tested and shown to produce wind analyses with field strengths of vorticity and divergence similar to the fields found by a separate analysis using the Endlich and Clark triangle method. At first glance, the final adjusted wind analysis appears to be identical to the preliminary wind field, but closer examination reveals small differences that result from the matching of vorticity and divergence between the measured fields and those defined by the final wind analysis. Examples of a preliminary wind field, its vorticity and divergence fields, its measured vorticity and divergence fields, and a final Schaefer-Doswell wind field are found in Appendix C.

Since this analysis scheme makes no assumptions about the relative strengths of the vorticity and divergence fields, and because it eliminates the direct manipulation of stream function and velocity potential, it was chosen as the most appropriate method for this study. The adopted wind analysis procedure based on vorticity and divergence constraints is as follows,

1) A Barnes scheme scanning only the closest 30 percent of the data points is used to produce a preliminary "u,v" wind analysis.

2) The vorticity and divergence fields for the preliminary wind analysis are determined by a polynomial fit in both the x and y directions to obtain directional gradients of u and v wind components. A description of the process and the theory behind obtaining gradients from an overlapping polynomial fit is found in appendix D.

3) The Endlich and Clark method is used for the calculation of point values of vorticity and divergence on which to base the measured fields of each. The optimum size and shape criteria for the triangles are determined in the next section.

4) A Barnes analysis of the Endlich and Clark vorticity and divergence point values is performed by scanning the closest 30 percent of the available data to produce the "measured" field of each.

5) The Schaefer-Doswell wind adjustment is performed on the preliminary analysis.

The last part of this section discusses the sensitivity testing of the adopted wind analysis scheme. However, for the actual testing, a slight deviation from the most accurate analysis procedure was used to enhance the quality of the test.

SENSITIVITY TESTING AND OPTIMIZATION OF THE ADOPTED PROCESS

The process for wind analysis using vorticity and divergence constraints, as described previously, requires that the constraining fields be defined on the basis of estimates obtained by the method described by Endlich and Clark (1963). Later discussion about the method by Ceselski and Sapp (1975) suggested that the shape of the triangles used for the estimation of vorticity and divergence may have an important effect on the quality of the estimates. Investigation during this study revealed that the size of the triangle also influences the triangle estimate.

To test the effect of the size and shape of the station triangles on the final accuracy of the adopted (vorticity/divergence) wind analysis procedure, a matrix of size and shape criteria for the Endlich and Clark triangles has been defined, and the performance of the full procedure was evaluated for each position of the matrix. The test matrix is comprised of nine shape criteria crossed with five size criteria.

The shape of the triangle is measured by the ratio of the largest vertex angle to the smallest vertex angle. In the test matrix, the maximum vertex angle ratio increases from 2.0 to 6.0 in increments of 0.5. It is difficult to quantify the triangle shape, or obliqueness, in terms of vertex angle ratio. There appears to be a direct relation between obliqueness and vertex angle ratio, but the relation does not appear to be linear.

The size of the triangle was measured in terms of its area in this study. In the test matrix, the maximum area criteria increases from 50,000 to 250,000 km^2 in increments of 50,000 km^2. With nine shape criteria and five size criteria, the test matrix requires 45 analysis tests for completion. For one analysis test with actual data, seven data sets are analyzed and errors are computed at the radiosonde stations within the test region. These error quantities are root mean square (RMS) and average absolute (AA) errors, which are calculated by comparing station observations with values obtained for the station locations from the final analysis using an overlapping polynomial interpolation in two dimensions (as described in Section 3).

For one analysis test with artificial data, six data sets are analyzed and errors are computed at station locations and at internal grid points. For this case, RMS and AA errors are calculated at the station locations in the same manner as for tests with actual data. For error analysis at the internal grid points, no interpolation scheme is required to match the analysis with the artificial data because data are available at all grid points. RMS and AA errors are calculated for the

20 internal grid points in a similar manner as for the station locations. As was explained earlier in this section, the results obtained from error analysis at the internal grid points are given more weight in the determination of the best analysis method because these test locations are evenly spaced and are present throughout the test region, and none of the errors determined by this test can be attributed to an interpolation of the final wind field.

The error quantities calculated for this test are not scaled to the data. Therefore, results from the actual data set should not be compared to results from the artificial data set because the variance of the data sets may differ significantly.

To enhance this test of the Endlich and Clark triangles and their effect in the final accuracy of the Schaefer-Doswell wind analysis scheme, the preliminary wind analysis was performed using a pure Barnes analysis scheme on separate "u" and "v" wind components. It was hoped that by using spatially consistent scale-dependent filtering for the preliminary analysis, a greater margin for improvement by the Schaefer-Doswell procedure would be allowed, and the effects from the varying triangle constraints would be more significant.

Error analyses for tests with actual data are shown in Appendix E, which include RMS and AA error responses for the test matrix. Both of these station location errors show minimums near the position on the matrix corresponding to a maximum vertex ratio of 4 to 5 and a maximum area of about 120,000 km^2. Error analyses for tests with artificial data based on station and grid point locations are shown in Appendix F, along with a figure showing the number of station triangles that could satisfy the requirements as determined by the test matrix. The station location RMS and AA errors show minimums around the position corresponding to a maximum vertex angle ratio of 3.5 and a maximum area of 100,000 km^2. The minimum RMS and AA errors based on grid point locations are found at a maximum angle ratio of 4 and maximum area of 100,000 km^2. These errors are nearly the same as those from station locations. The results seem to indicate that the excessively oblique triangles should be rejected even though this reduces the number of triangles on which the vorticity and divergence forcing fields are based.

To test the sensitivity of the wind analysis procedure to the type of gridding method used on the Endlich and Clark triangle values, the previously mentioned test with artificial data was repeated using a pure Barnes scheme instead of the modified version. The error analyses in Appendix G indicate that in this case, the minimum errors are slightly larger and their locations are shifted toward smaller values of the vertex angle ratio. A balance seems to exist between the greater smoothing of the pure Barnes gridding and the more complex structure of the triangle centroid data fields produced from smaller triangles.

The test results from the artificial data set seem to indicate that there is a point of diminishing return in respect to the number of tri-

angles produced for the vorticity and divergence point values. While a large number of centroid estimates is helpful for the determination of the forcing fields, the confidence placed on oblique triangle estimates should be less than that placed on more nearly equilateral ones. When the increased computing time involved in the production of these unreliable estimates is considered, the optimum number of triangles is reduced further. After considering this factor, the author concluded that the most efficient triangle criterion is for the maximum vertex angle ratio to be limited to about 3.0 and for the maximum area to be 100,000 km^2.

An error evaluation of the optimum wind analysis procedure, defined earlier in this section, was performed for the most accurate portion of the test matrix. The error results, shown in Table 5, show that from the Schaefer-Doswell procedure using the most accurate scheme to perform the preliminary wind analysis, the smallest obtainable grid point RMS error is about 1.4 m/s.

Table 5 - ERROR RESULTS FOR THE ADOPTED WIND ANALYSIS PROCESS

TRIANGLE CRITERION		(stations)		(grid points)	
ANGLE RATIO	SIZE	RMS	AA	RMS	AA
2	2	1.213 m/s	1.100 m/s	1.467 m/s	1.244 m/s
2	3	1.253	1.156	1.570	1.343
2	4	1.353	1.258	1.664	1.440
3	2	1.184	1.097	1.494	1.267
3	3	1.193	1.108	1.537	1.309
3	4	1.258	1.174	1.585	1.366
4	2	1.203	1.115	1.487	1.252
4	3	1.188	1.097	1.504	1.280
4	4	1.295	1.213	1.596	1.385
5	2	1.147	1.073	1.409	1.192
5	3	1.157	1.074	1.473	1.255
5	4	1.254	1.170	1.571	1.367
6	2	1.182	1.102	1.443	1.220
6	3	1.204	1.116	1.503	1.287
6	4	1.242	1.155	1.561	1.361
7	2	1.232	1.143	1.470	1.249
7	3	1.217	1.130	1.504	1.292
7	4	1.258	1.170	1.568	1.371

RMS = root mean square error

AA = average absolute error

SECTION 5

RESULTS AND DISCUSSION

TEMPORAL INTERPOLATION FOR NEROS

Hourly wind vector grids across the study region are required as input for the NEROS model. Such hourly data cannot be obtained by observation. Therefore, a technique for the estimation of wind fields at intermediate times (i.e., temporal interpolation) is required.

For this study, intermediate time wind values were obtained by linear interpolation of recorded radiosonde observations, which were generally taken at 12 hour intervals. Some special observations were made at the intermediate 6 hour times at particular stations as a part of the NEROS study, but these were made only during limited test periods.

One such test period was from 0000 GMT August 3, 1979 to 0000 GMT August 6, 1979. During this time, special 0600 GMT and 1800 GMT observations were taken at seven standard radiosonde launching sites in the northeastern United States. Unfortunately, the technicians at certain sites were unable to begin or complete some of their observations during this period, but the data set that was obtained provides a measure for judging temporal interpolation techniques.

The idea of using linear interpolation in time to estimate the transient properties of the highly non-linear atmosphere may seem unrewarding. However, when the greater complexity and nonuniqueness of curvilinear interpolation schemes is understood, the more straightforward alternative becomes more attractive.

When attempting to estimate fields or arrays of wind values at intermediate times, in addition to deciding whether to use linear or curvilinear time interpolation, the investigator must decide whether to temporally interpolate the data at the observation site and proceed with the spatial gridding processes or to produce the spatial grids for the times when data are available and then temporally interpolate the grid point values. To answer this question, an investigation was conducted using the data that were collected during the previously mentioned test period between 0000 GMT August 3, 1979 and 0000 GMT August 6, 1979.

First, linear time interpolation was used to estimate 0600 GMT and 1800 GMT wind observations at the 850, 700, and 500 mbar levels, wherever the adjacent 0000 GMT and 1200 GMT observations were available among the

Table 6 - ERROR RESULTS FOR TIME INTERPOLATION PROCEDURE ONE

Pressure Level	Scaled RMS Error	Scaled Average Absolute Error
850 mb.	.6989	.5318
700 mb.	.6662	.5615
500 mb.	.5164	.3874
Overall Scaled RMS Error =		.6359
Overall Scaled Average Absolute Error =		.4979

Table 7 - ERROR RESULTS FOR TIME INTERPOLATION PROCEDURE TWO

Pressure Level and Analysis Time	Scaled RMS Error	Scaled Average Absolute Error
850 mb. 0000 & 1200 GMT	.374	.256
850 mb. 0600 & 1800 GMT	.671	.495
700 mb. 0000 & 1200 GMT	.551	.251
700 mb. 0600 & 1800 GMT	.618	.519
500 mb. 0000 & 1200 GMT	.185	.144
500 mb. 0600 & 1800 GMT	.460	.353
Overall Scaled RMS Error (0000 & 1200 GMT) =		.401
Overall Scaled RMS Error (0600 & 1800 GMT) =		.591
Overall Scaled Average Absolute Error (0000 & 1200 GMT) =		.217
Overall Scaled Average Absolute Error (0600 & 1800 GMT) =		.457

sites participating in the data collection experiment. These simple linear estimates were statistically compared to their corresponding observed winds at 0600 GMT and 1800 GMT. The error results from this method are shown in Table 6. Without the influence of any spatial gridding on values for the station locations, these statistics were used as a measure to judge a second procedure.

The second procedure entailed the spatial gridding of the same set of wind data at all 0000 GMT and 1200 GMT observation times during the period, regardless of how many observations might have been missed at each time. A modified Barnes technique using the closest 30 percent of the data points was used to estimate each grid point value. Scaling parameters for the technique were set to provide a 50 percent wave response at the 800 km wavelength. After these grids were produced, each grid point value was linearly interpolated in time to get 0600 GMT and 1800 GMT grids.

To check the accuracy of this procedure, an overlapping polynomial estimation process was used in two dimensions to get station location values from each grid at data times and at the intermediate times. Then these values were compared with the actual observed values for both times, whenever such observations were available. The statistical error results for this procedure are shown in Table 7.

These error results were influenced by three factors that did not influence the error results for the first procedure. First, because missing data for the 0000 GMT and 1200 GMT tests did not prevent the second procedure from providing time interpolation estimates, more test cases were provided, thereby strengthening the statistical significance of the error results. Next, because the second procedure included temporal and spatial interpolation, while the first used only temporal interpolation, additional variability is incorporated into the error results for the second procedure. Finally, because a second spatial interpolation process was required to provide station location values and error results for the second procedure, more variability was added to its error results.

Despite the effect of these three normally detrimental factors, the statistical accuracy of the second procedure is greater than that of the first for intermediate station wind estimates. Not only does the second procedure appear more accurate from these statistics, it is able to produce 0600 GMT and 1800 GMT estimates for every station location, regardless of whether 0000 GMT or 1200 GMT observations were missed. When such observations were missed, if an interpolation through 24 or more hours was performed in the first procedure, the resulting errors are likely to have been considerably larger.

In conclusion, although the second procedure produced statistically more accurate results for the intermediate time estimates, a considerable increase in error occured compared to the errors at actual observation times. This increase seems to indicate that regardless of the order of

the time and space interpolations, linear time interpolation falls short of optimally estimating transient wind values. During this investigation, a third procedure was studied in which a cubic spline was used for grid point time interpolation. Lack of control over the spatial continuity of grid point time derivatives at data times caused the intermediate grids to displayed great disorder and noise. More control over the time derivatives in the curvilinear time interpolation of grid points may provide acceptable wind fields for intermediate times, but development of such a technique is beyond the scope of this investigation.

USER GUIDE TO NEROS WIND ANALYSIS SOFTWARE

The software package that was developed as a result of this investigation is cataloged on the UNIVAC 1183 on the NEROS mountable disk pack NCC011, under the file name "NEROS*RUSSWINDANAL." This package consists of 13 elements, two of which are the externally accessable subroutines: "WINDS1" and "WINDS2." Calling WINDS1 produces a 7 by 6 grid of "u" and "v" wind components by the simpler separate component analysis method using a modified Barnes scheme that scans only the closest 30 percent of the data points during each grid point value estimation. "WINDS2" produces the same output by the more complicated Schaefer-Doswell procedure that was adopted during this investigation. In each case, scaling parameters are set to provide a 50 percent wave response at the 800 km wavelength for every spatial analysis, and the spatial definition of the output grid is identical to that of the computational grid discussed in Section 3.

For both subroutines, no variables are passed in the CALL statement. Rather, Input/Output is by way of two COMMON blocks as follows.

```
COMMON /INPUT/ STLAT(25),STLON(25),UST(25),VST(25),NUM
COMMON /OUTPUT/ U(7,6),V(7,6)
```

where,

STLAT(N) = the latitude at the Nth wind observation
STLON(N) = the longitude at the Nth wind observation
UST(N) = the u-component of the Nth wind observation
VST(N) = the v-component of the Nth wind observation
NUM = the total number of wind observations (25 maximum)
U(I,J) = the u-component estimate for grid position "I,J"
V(I,J) = the v-component estimate for grid position "I,J"

The collection and validation of input wind data for this analysis package is the responsibility of the user. The input data does not have specific requirements with respect to the number of observations or the units used to express the wind. However, there should be at least 15 wind observations obtained in and around the NEROS region to insure a realistic wind analysis over the entire region. This data requirement depends on the spatial configuration of the observation points and cannot be analytically described. Any system of units may be used for the input

wind components because the units are transparent to the analysis procedure and the output units will correspond to any units used for input. Currently, the number of input data points is limited to 25. If expansion becomes necessary, it will not present a significant software modification problem. To use "WINDS1" or "WINDS2" in a regular subroutine call, the statement "LIB NEROS*RUSSWINDANAL." must be included in the "@MAP" procedure which creates the calling program.

REFERENCES

Baker, W. E., 1983: Objective analysis and assimilation of observational data from FGGE, Mon. Wea. Rev., 107, (4): 458-476.

Barnes, S. L., 1964: A technique for maximizing details in numerical weather map analysis, J. Appl. Meteor., 3: 396-409.

Barnes, S. L., 1973: Mesoscale objective map analysis using weighted time series observations. NOAA Tech. Memo. ERL NSSL-62, 60 pp.

Bellamy, J. C., 1949: Objective calculations of divergence, vertical velocity, and vorticity, Bull. Amer. Meteor. Soc., 30, (2): 45-49.

Belt, C. L., and H. E. Fuelberg, 1982: The effects of random errors in rawinsonde data on derived kinematic quantities, Mon. Wea. Rev., 110: 91-101.

Bleck, R. and P. L. Haagenson, 1968: Objective analysis on isentropic surfaces, NCAR Tech. Notes NCAR-TN-39: 19-26.

Ceselski, B. F. and L. L. Sapp, 1975: Objective wind field analysis using line integrals, Mon. Wea. Rev., 103, (2): 89-100.

Chien, H. and P. J. Smith, 1973: On the estimation of kinematic parameters in the atmosphere from radiosonde wind data, Mon. Wea. Rev., 101, (3): 252-261.

Cressman, G. P., 1959: An operational objective analysis system, Mon. Wea. Rev., 87, (10): 367-374.

Doswell, C. A., 1977: Obtaining meteorologically significant surface divergence fields through the filtering property of objective analysis, Mon. Wea. Rev., 105: 885-892.

Endlich, R. M. and J. R. Clark, 1963: Objective computation of some meteorological quantities, J. Appl. Meteor., 2: 66-81.

Endlich, R. M. and R. L. Mancuso, 1964: A direct method of stream function computation, Tellus, 16: 32-39.

Fritsch, J. M., E. L. Mazaginer, and C. F. Chappell, 1980: Analytical initialization for three-dimensional numerical models, J. Appl. Meteor., 19: 809-818.

Hawkins, H. F. and S. L. Rosenthal, 1965: On the computation of stream functions from the wind field, Mon. Wea. Rev., 93, (4): 245-252.

Kurihara, Y., 1961: Accuracy of winds aloft data and estimation of error in numerical analysis of atmospheric motions, J. Meteor. Soc. Japan, 39: 331-345.

Maddox, R. A., 1980: An objective technique for separating macroscale and mesoscale features in meteorological data, Mon. Wea. Rev., 108: 1108-1121.

Schaefer, J. T., and C. A. Doswell, 1979: On the interpolation of a vector field, Mon. Wea. Rev., 107, (4): 458-476.

Shuman, F. G., 1957: Numerical methods in weather prediction: II. smoothing and filtering, Mon. Wea. Rev., 85, (11): 357-361.

Swarztrauber, P. N., 1974: The direct solution of the discrete poisson equation on the surface of a sphere, J. of Comput. Phy., 15: 46-54.

Whittaker, T. M. and R. A. Petersen, 1977: Objective cross-sectional analyses incorporating thermal enhancement of the observed winds, Mon. Wea. Rev., 105: 147-153.

Williams, R. J., 1976: Surface parameters associated with tornadoes, Mon. Wea. Rev., 104, (5): 540-545.

APPENDIX A - SURFACE AND 700 MBAR CHARTS

(0000 GMT August 3, 1979, through 0000 GMT August 6, 1979)

Reproduced from
best available copy.

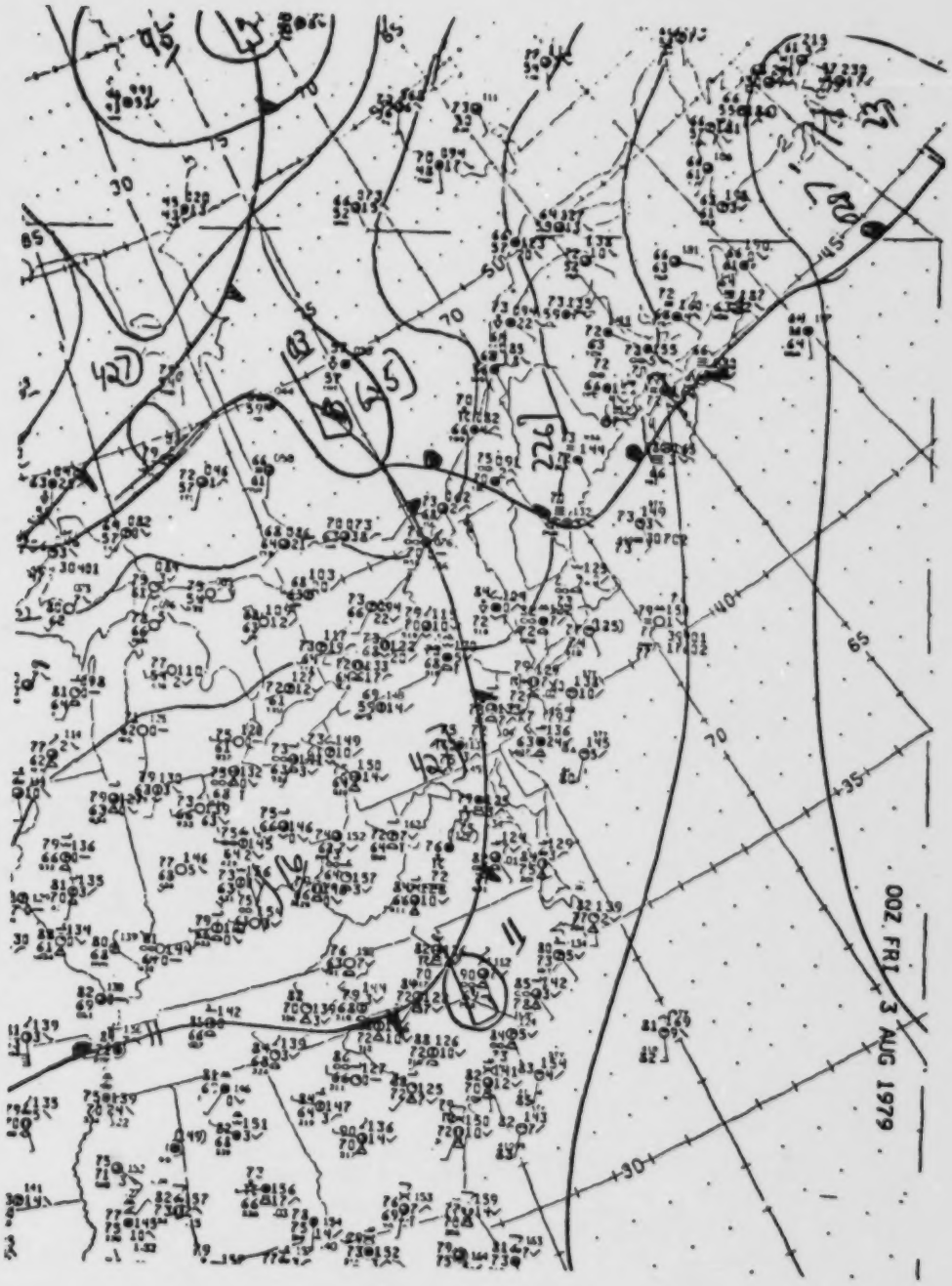

Surface Chart for 0000 GMT August 3, 1979

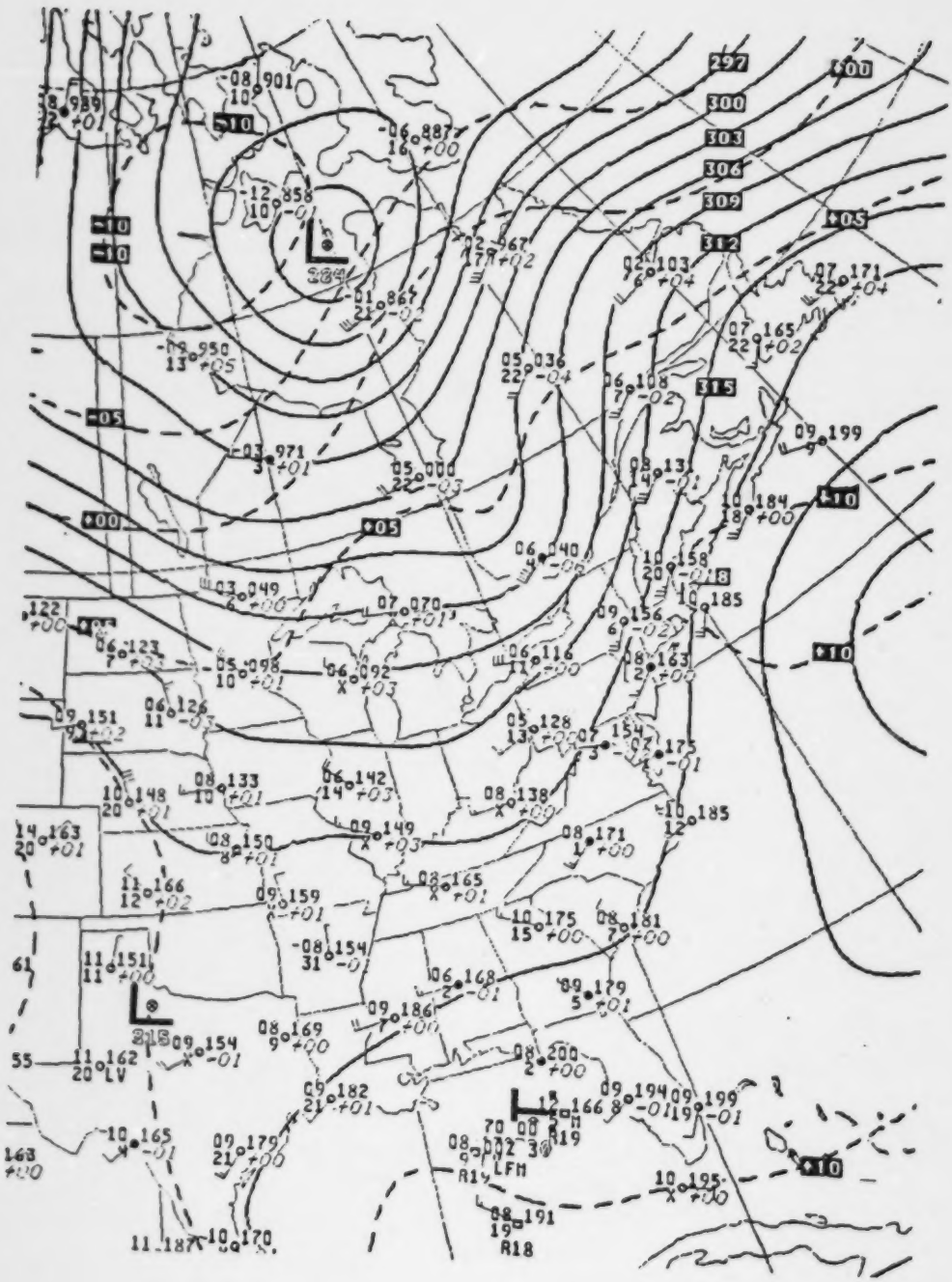

700 mbar Chart for 0000 GMT August 3, 1979

Reproduced from
best available copy.

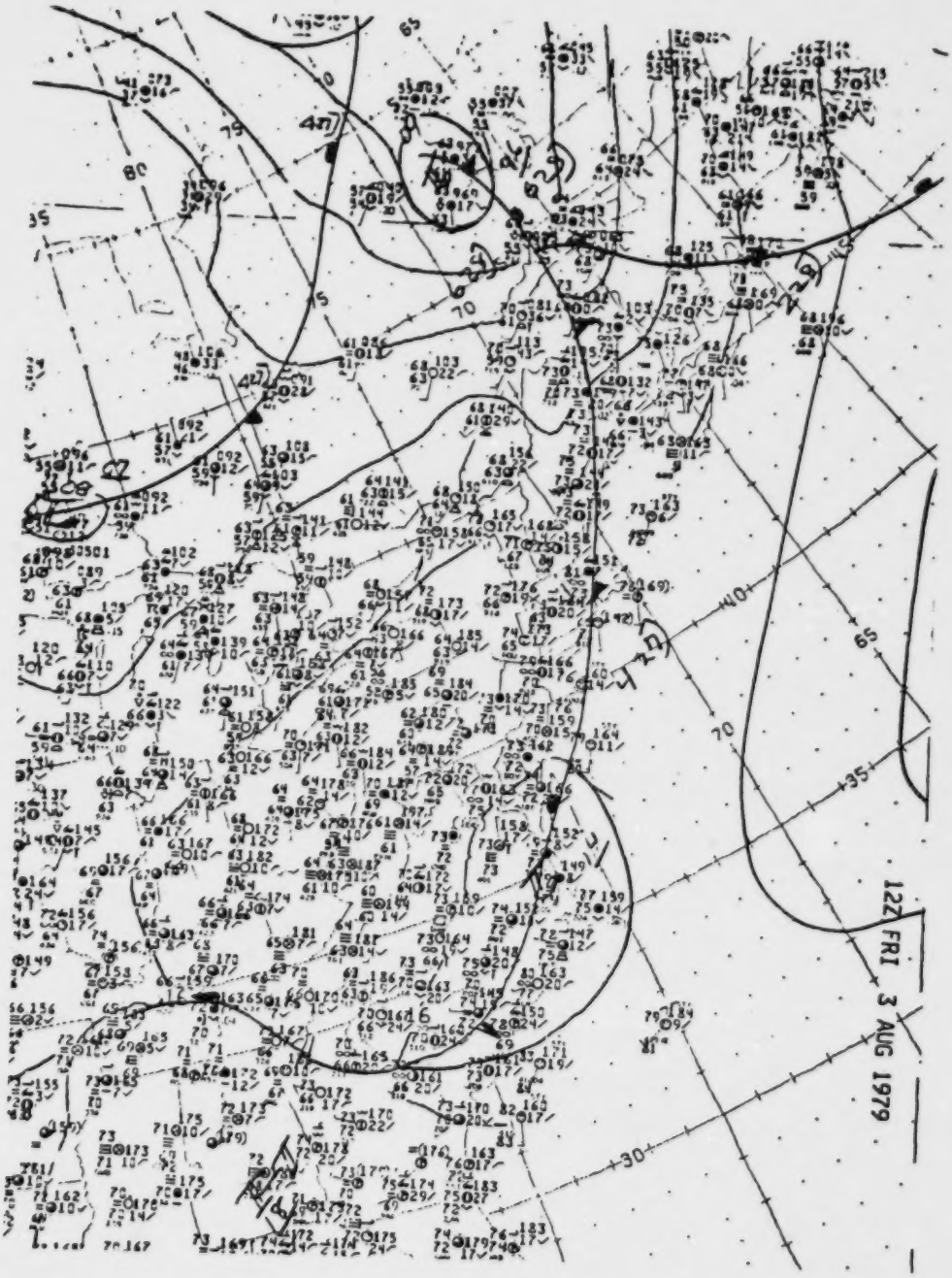

Surface Chart for 1200 GMT August 3, 1979

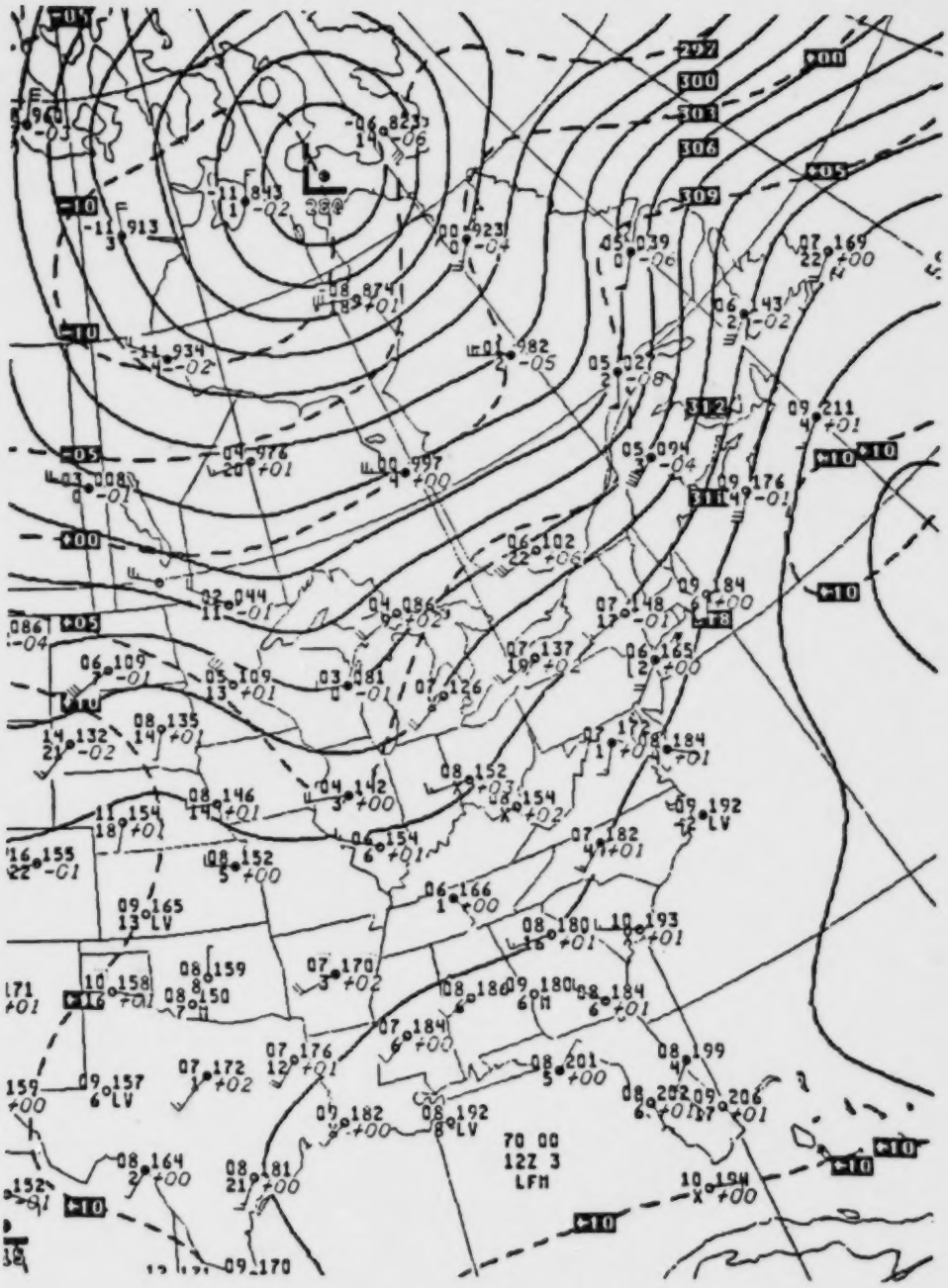

700 mbar Chart for 1200 GMT August 3, 1979

Reproduced from
best available copy.

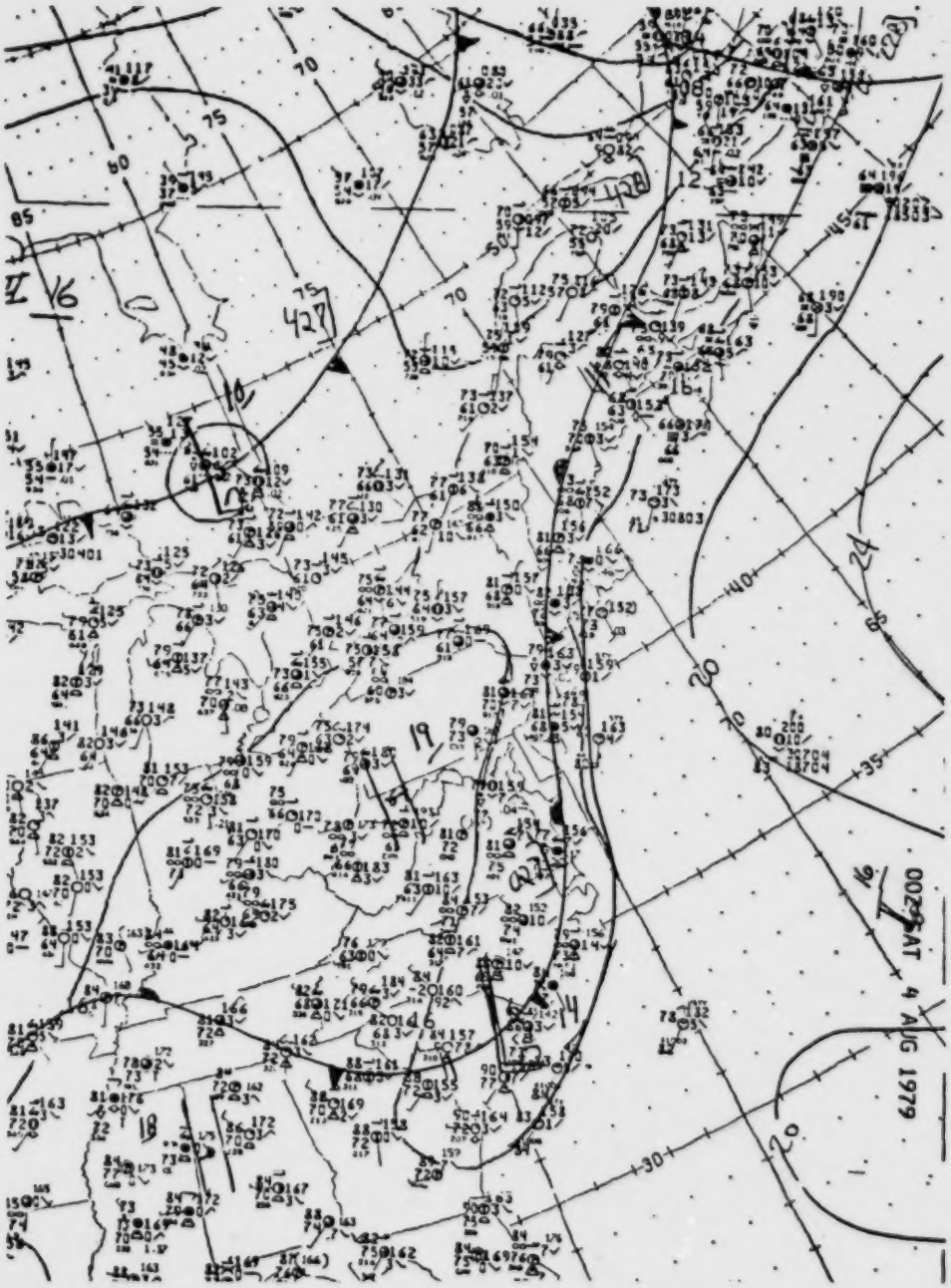

Surface Chart for 0000 GMT August 4, 1979

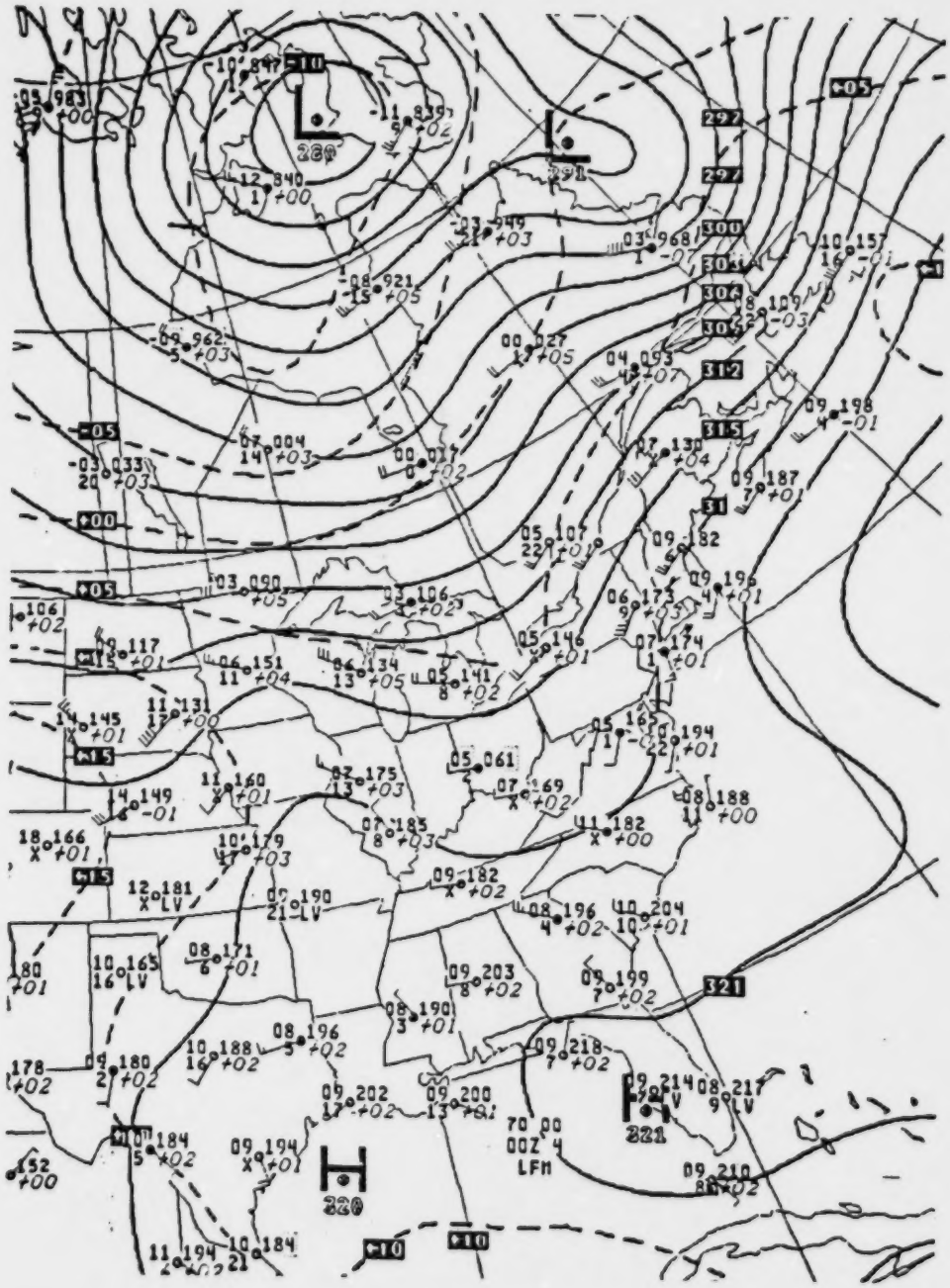

700 mbar Chart for 0000 GMT August 4, 1979

Reproduced from
best available copy.

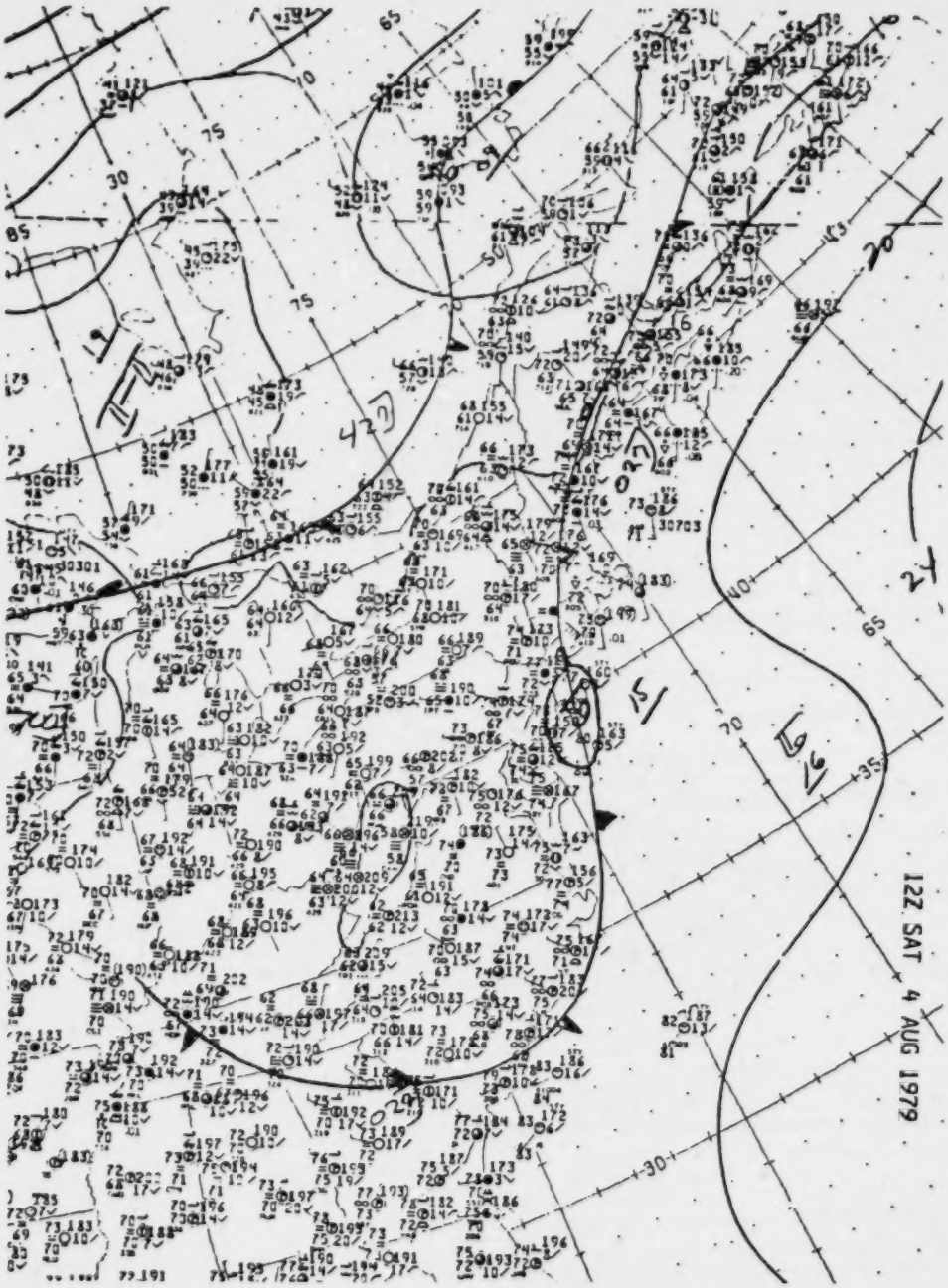

Surface Chart for 1200 GMT August 4, 1979

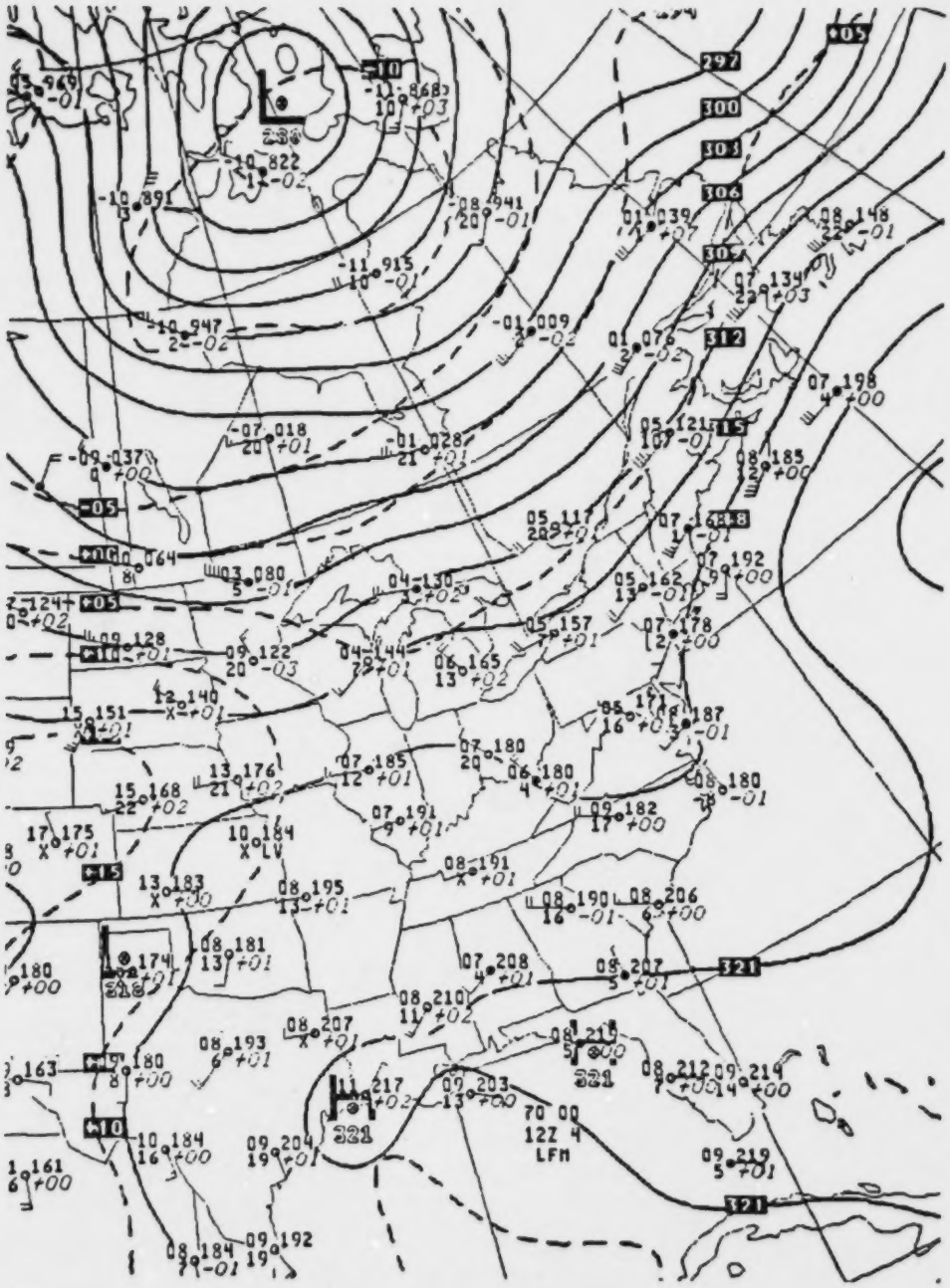

700 mbar Chart for 1200 GMT August 4, 1979

Reproduced from
best available copy.

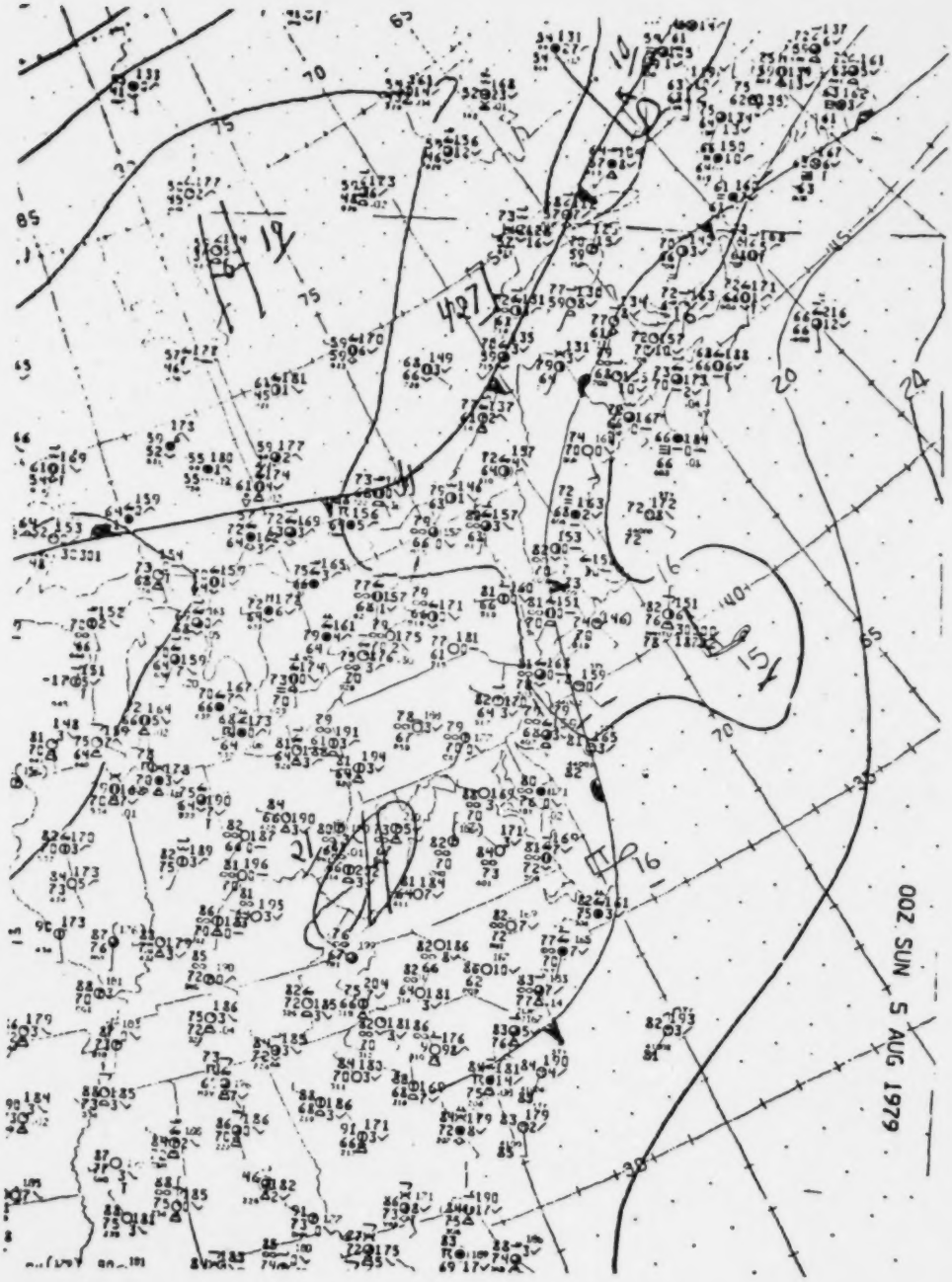

Surface Chart for 0000 GMT August 5, 1979

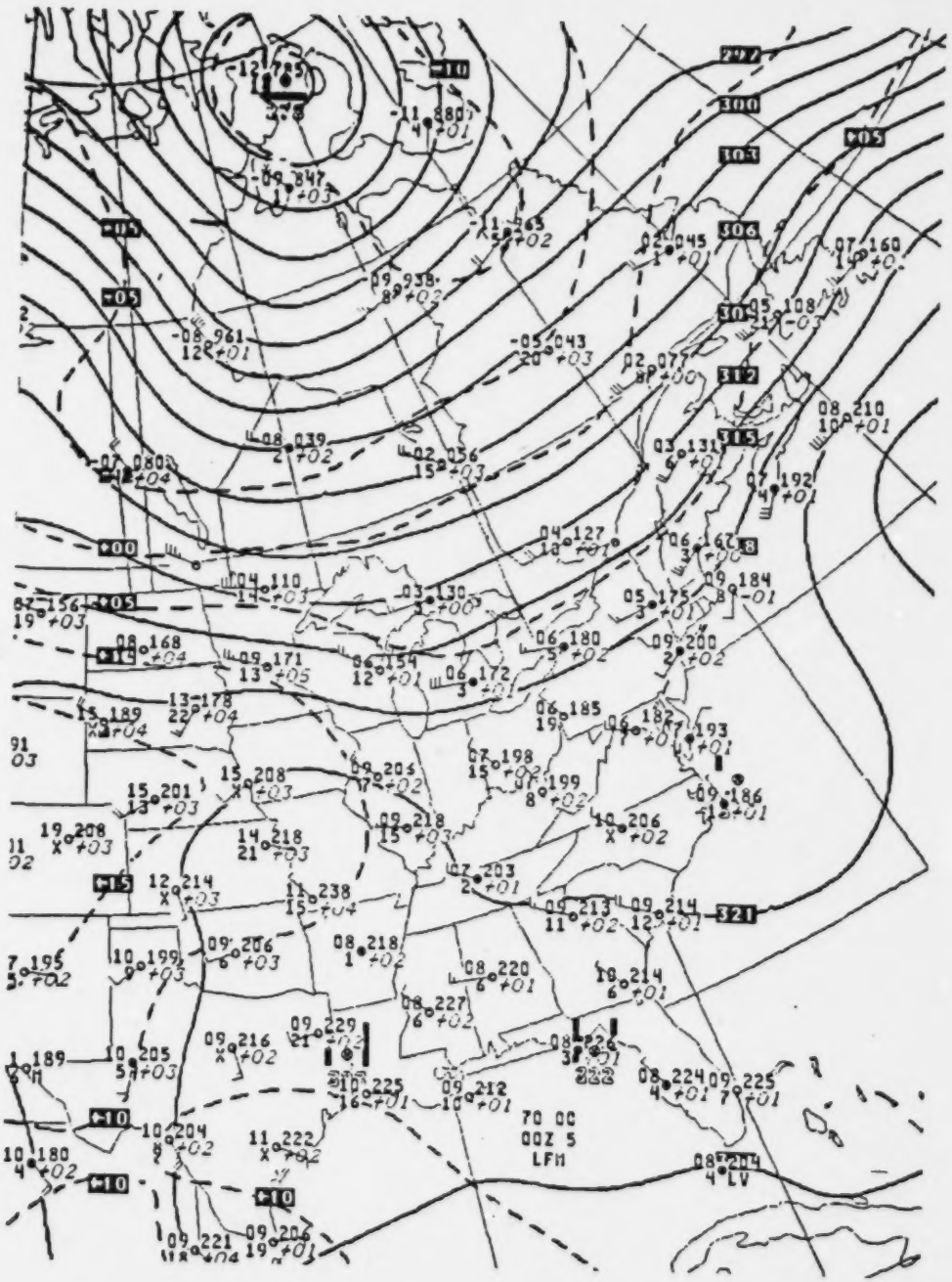

700 mbar Chart for 0000 GMT August 5, 1979

Reproduced from
best available copy.

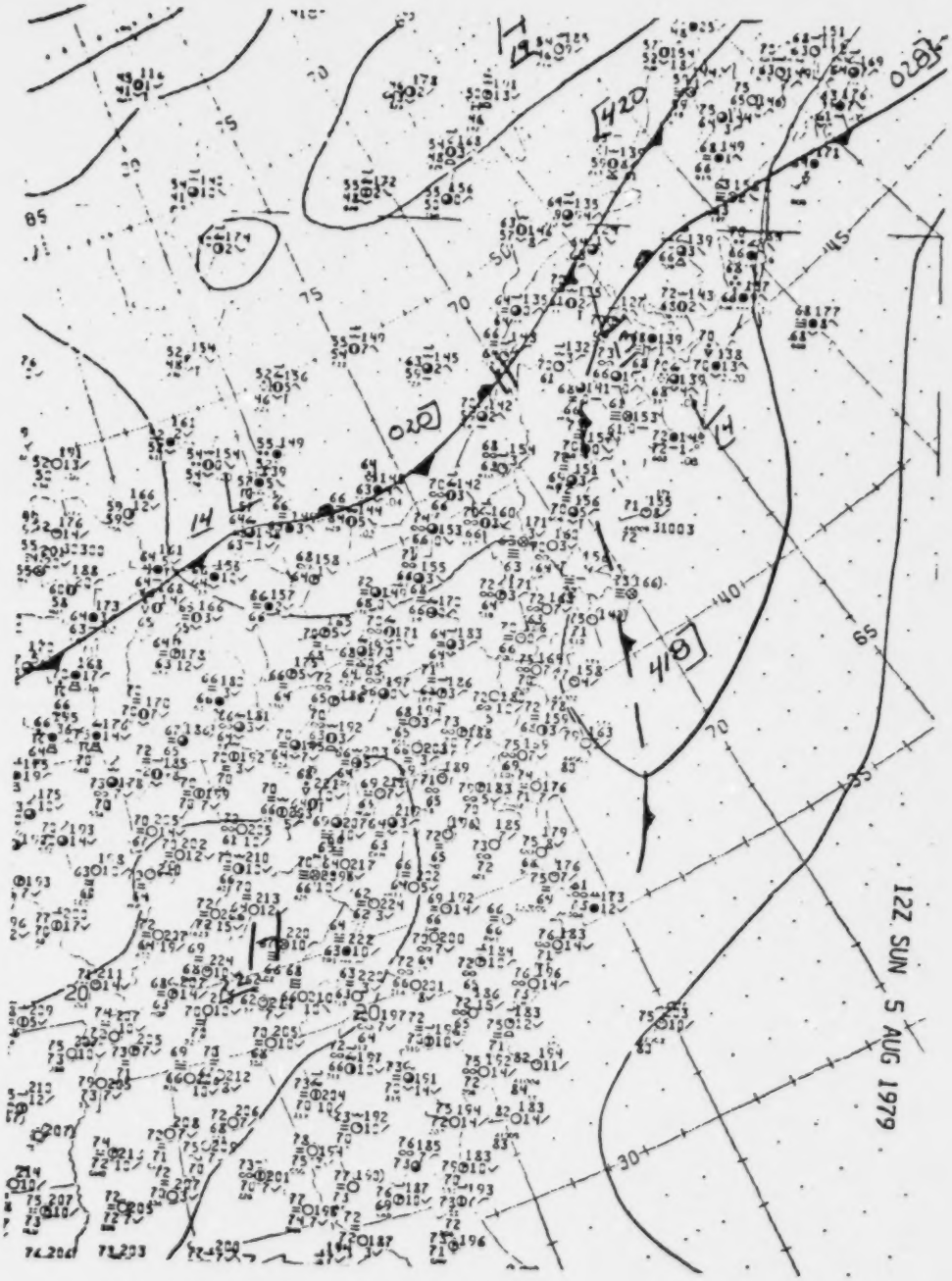

Surface Chart for 1200 GMT August 5, 1979

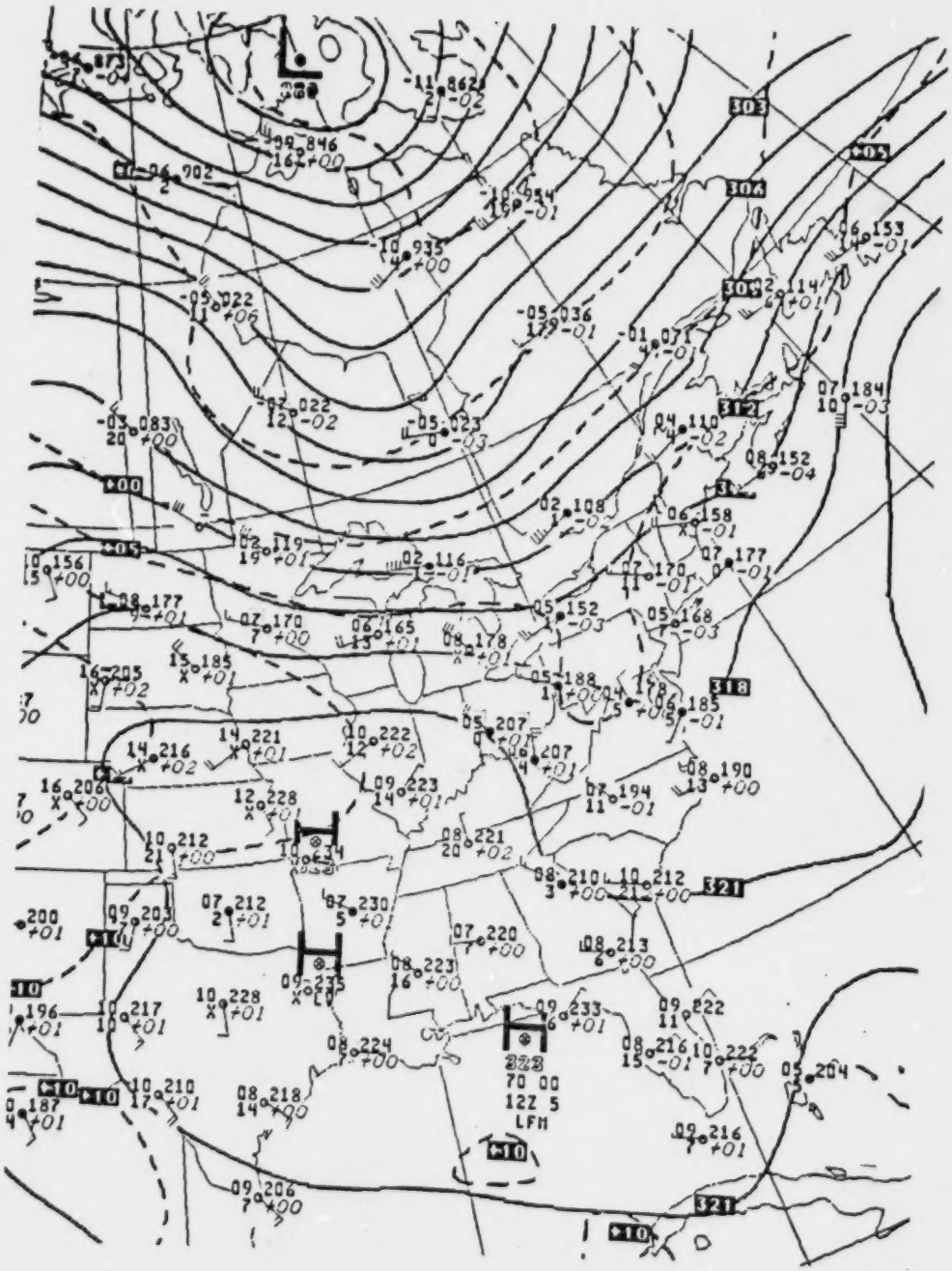

700 mbar Chart for 1200 GMT August 5, 1979

Reproduced from
best available copy.

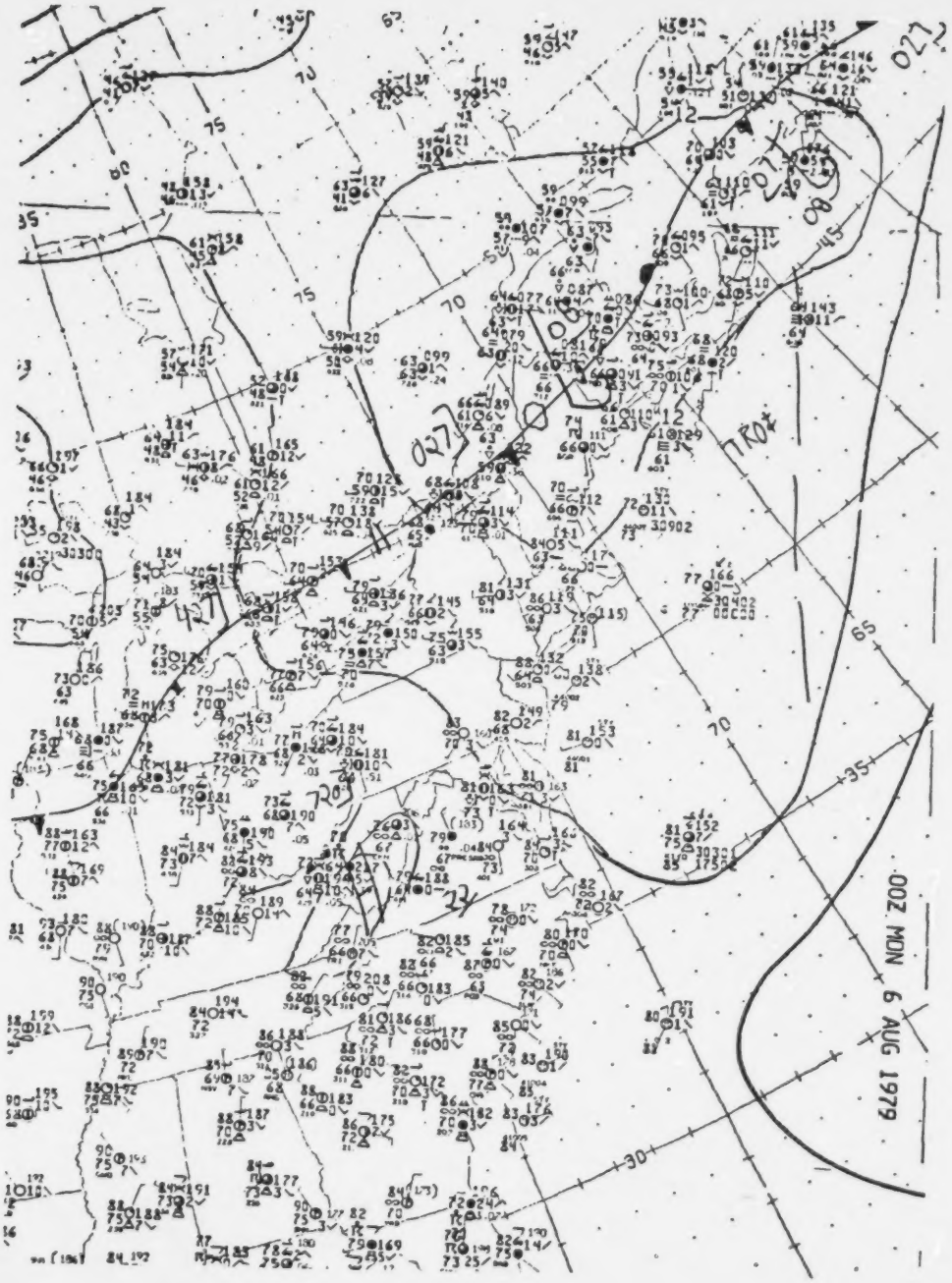

Surface Chart for 0000 GMT August 6, 1979

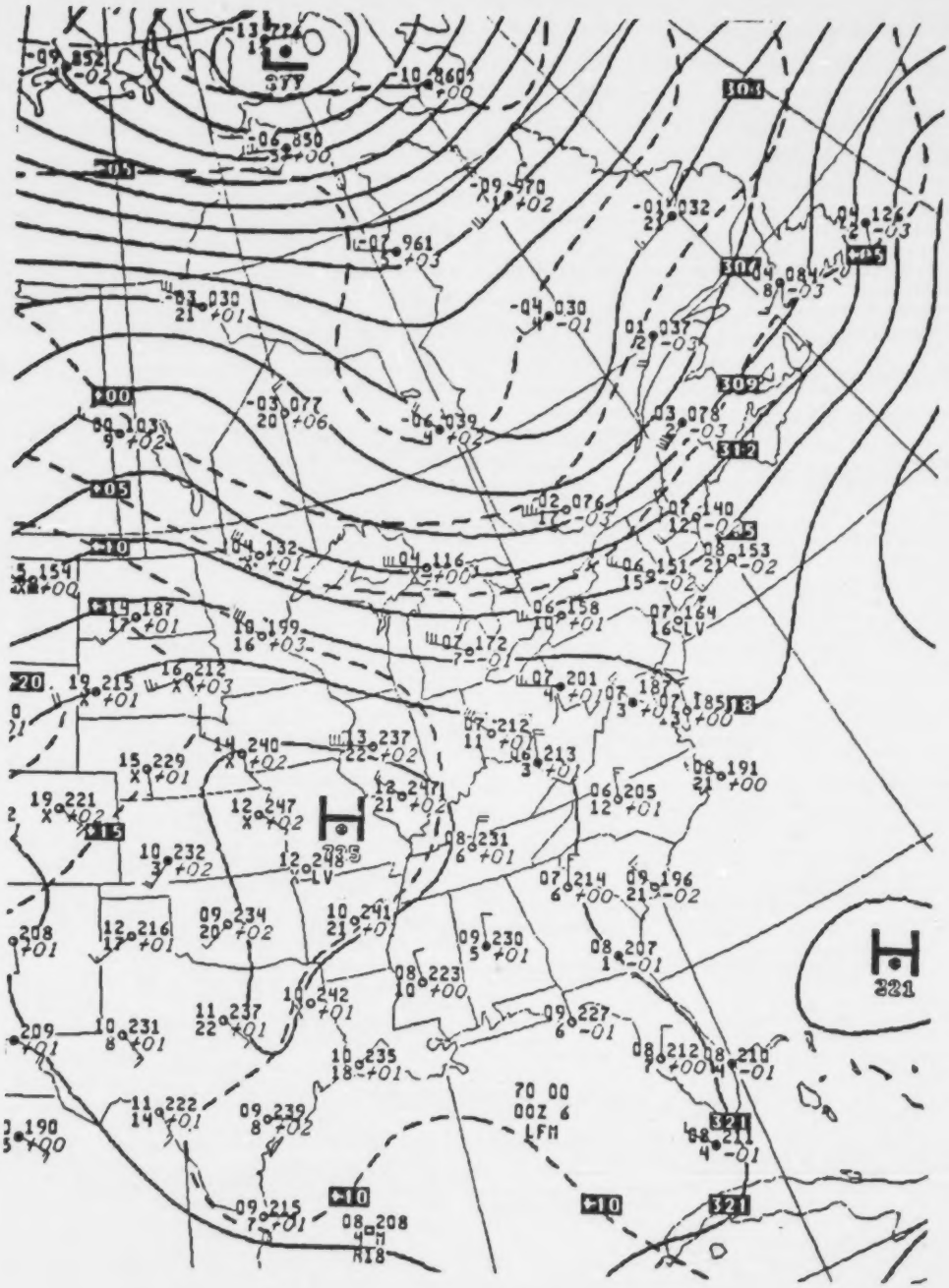

700 mbar Chart for 0000 GMT August 6, 1979

APPENDIX B - ARTIFICIAL FIELDS OF 700 MBAR HEIGHT AND GRADIENT WIND

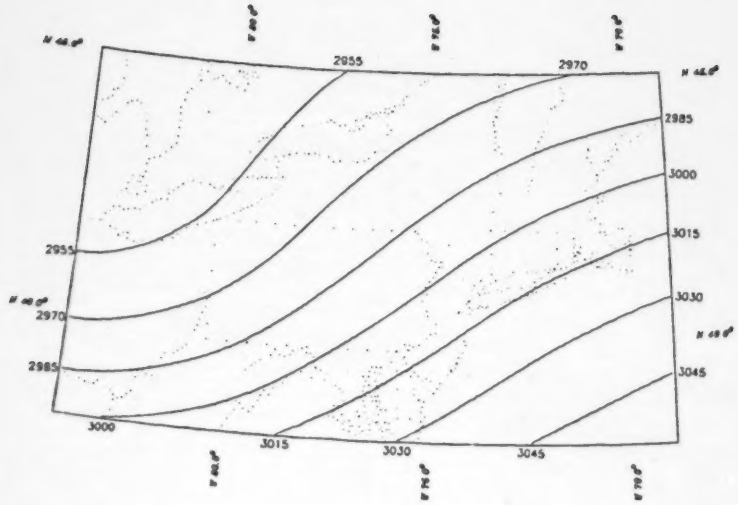

700 mbar Height Field Number One (meters)

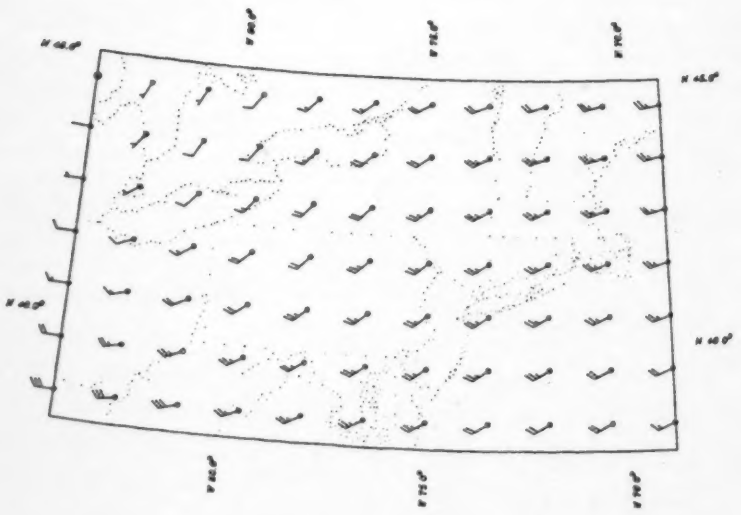

700 mbar Gradient Wind Field Number One

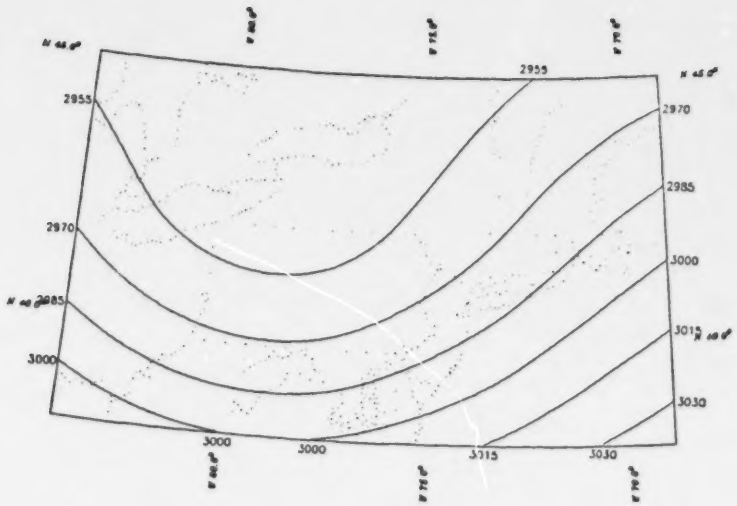

700 mbar Height Field Number Two (meters)

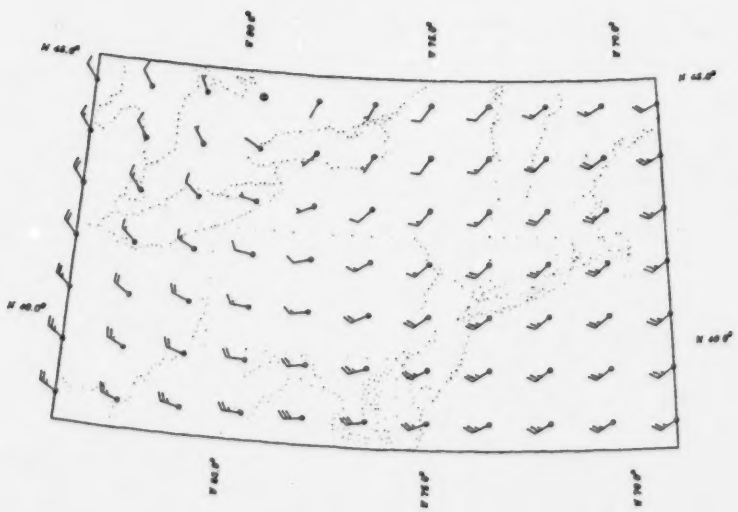

700 mbar Gradient Wind Field Number Two

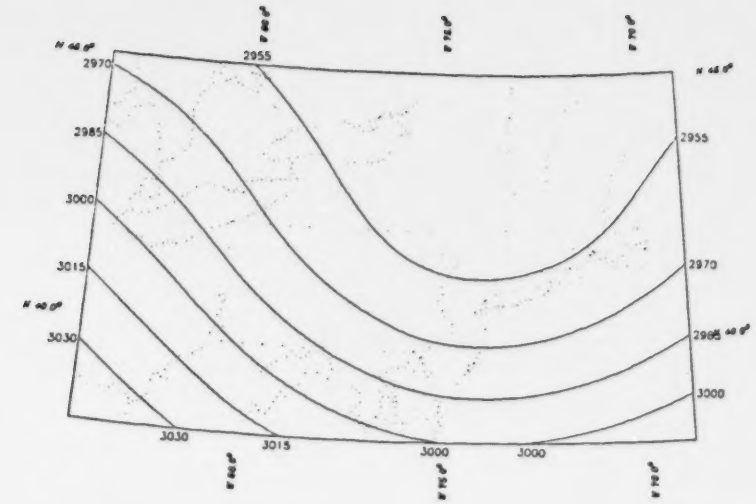

700 mbar Height Field Number Three (meters)

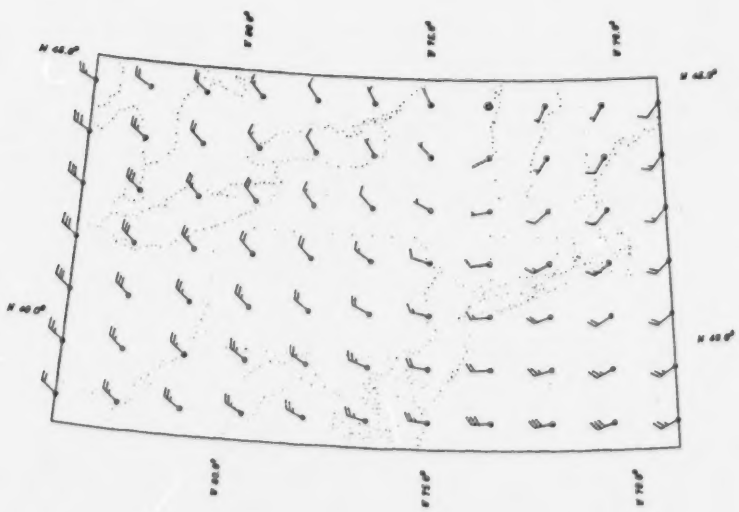

700 mbar Gradient Wind Field Number Three

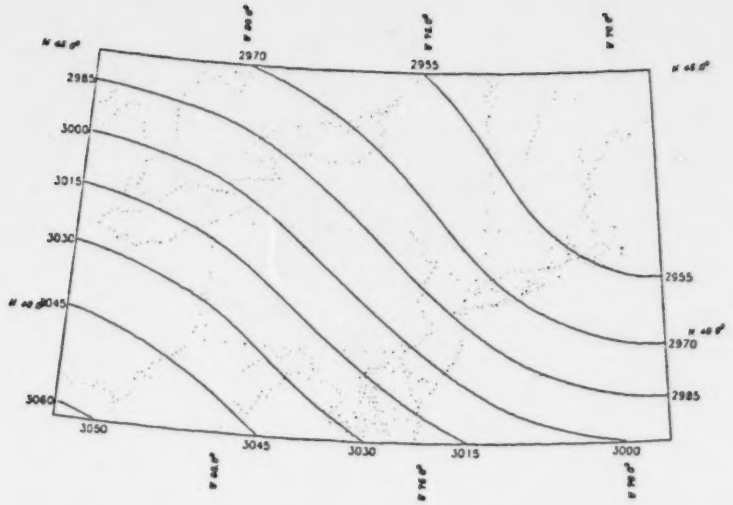

700 mbar Height Field Number Four (meters)

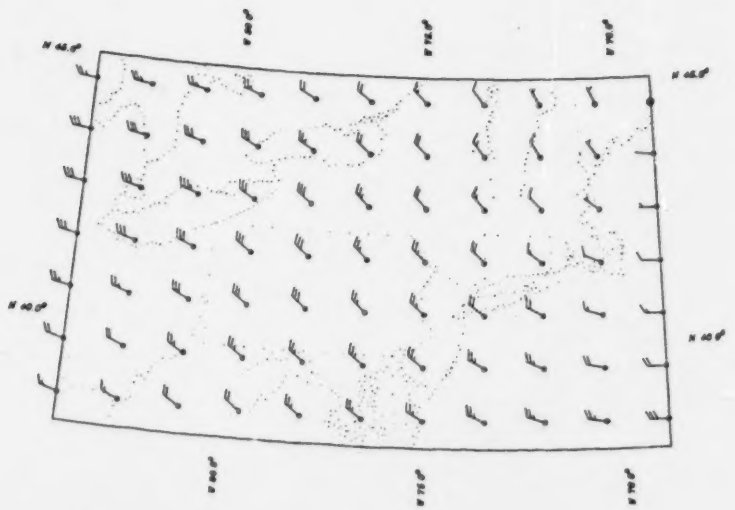

700 mbar Gradient Wind Field Number Four

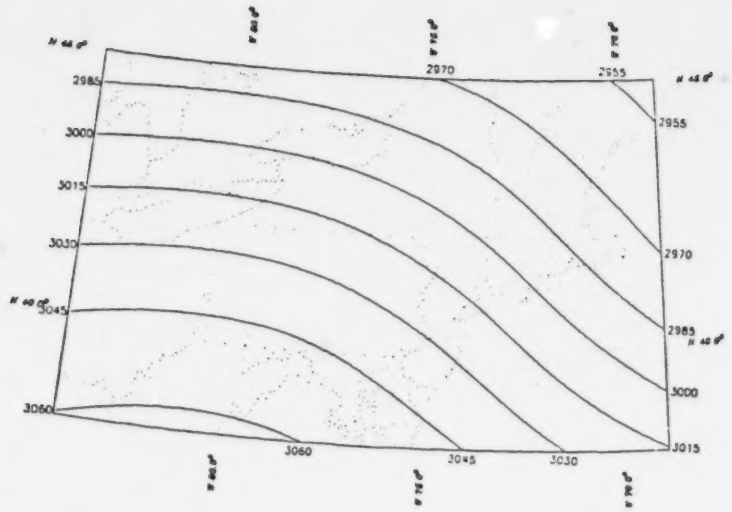

700 mbar Height Field Number Five (meters)

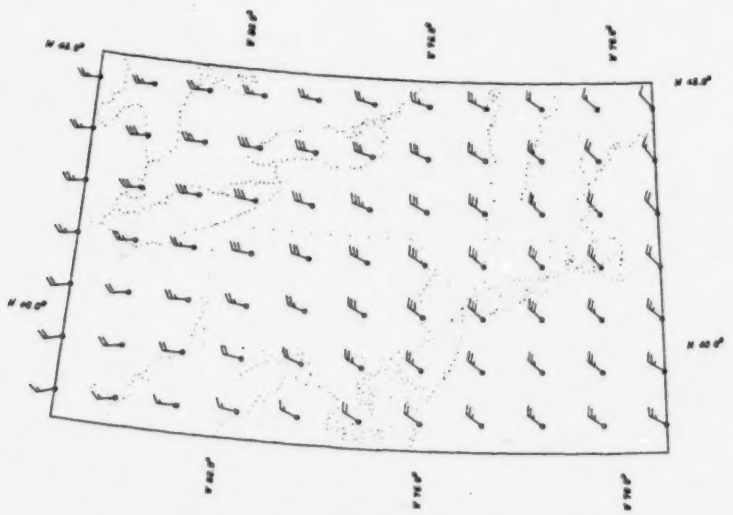

700 mbar Gradient Wind Field Number Five

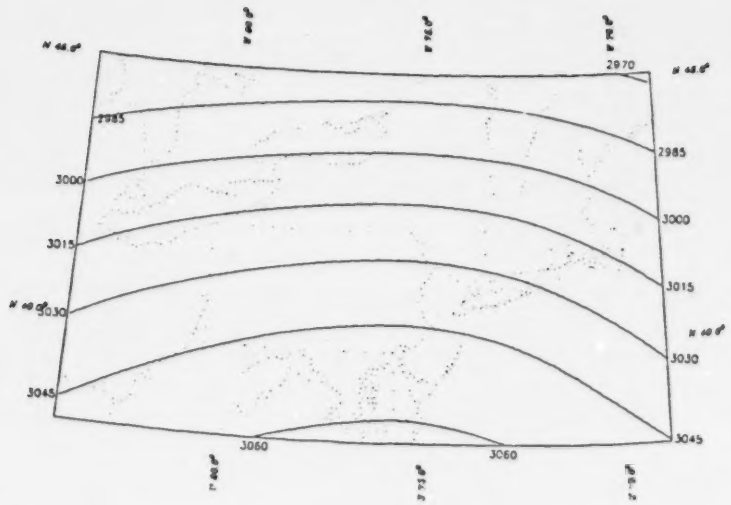

700 mbar Height Field Number Six (meters)

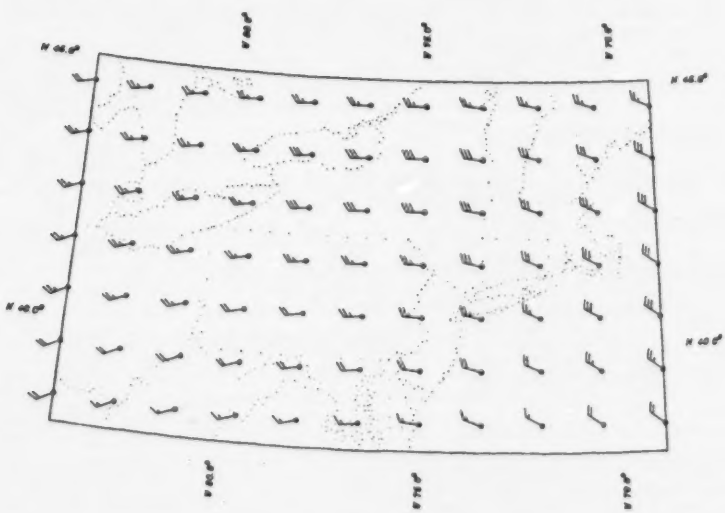

700 mbar Gradient Wind Field Number Six

APPENDIX C - EXAMPLES OF PRELIMINARY, MEASURED, AND FINAL ANALYSIS FIELDS FROM THE SCHAEFER-DOSWELL PROCEDURE

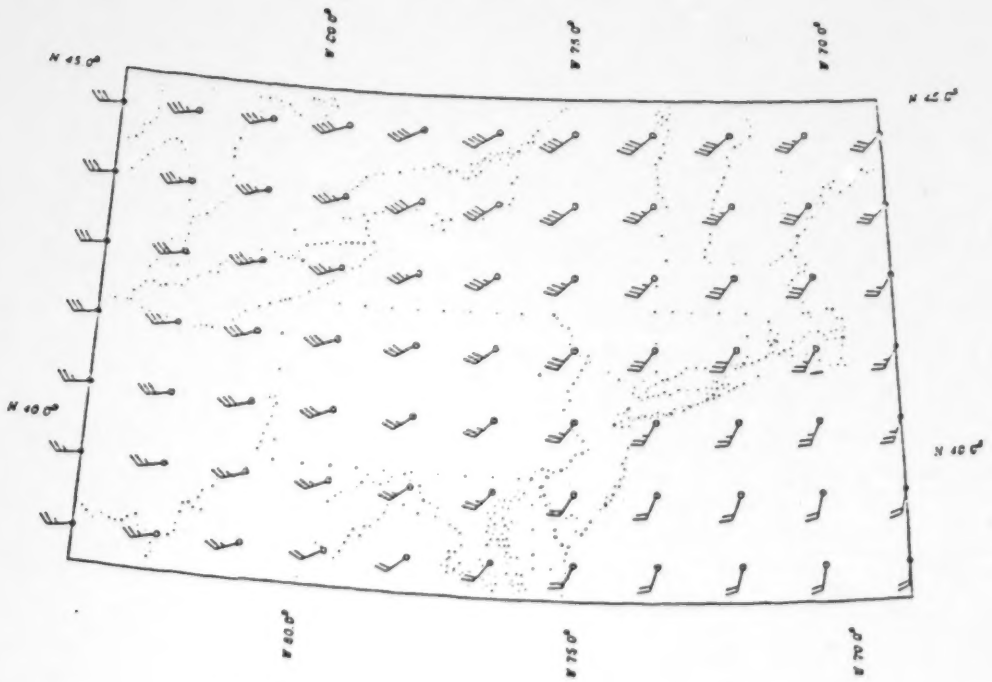

Preliminary Wind from Barnes Analysis
of separate U and V components

STA.	LAT/LON	UST/VST		U/V		DIFF
72493	38.95 77.45	7.59	7.89	7.14	6.66	1.58
72425	38.37 82.55	13.43	3.69	11.29	2.92	2.24
72518	42.75 73.80	14.21	14.21	11.25	12.01	3.69
72528	40.50 80.22	15.97	5.81	12.88	5.27	3.14
72528	42.93 78.73	17.85	6.58	15.66	7.49	2.41
72536	43.65 79.32	10.61	12.64	11.28	12.29	.76
74486	40.65 73.78	5.66	12.14	6.68	10.76	1.72
74494	41.67 69.97	6.55	12.04	7.21	11.58	.52

WIND FIELD VARIANCE = 5.38

WIND FIELD RMS = 2.25

WIND FIELD AVG. ERROR = 2.01

Error Analysis

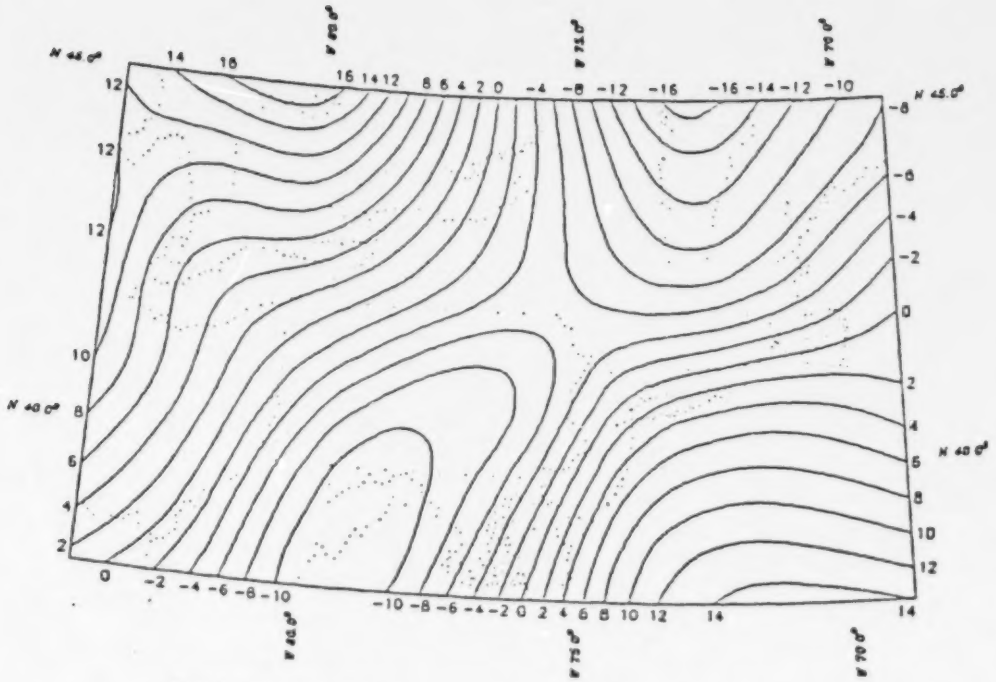

Preliminary Divergence Field (10-6 sec-1)

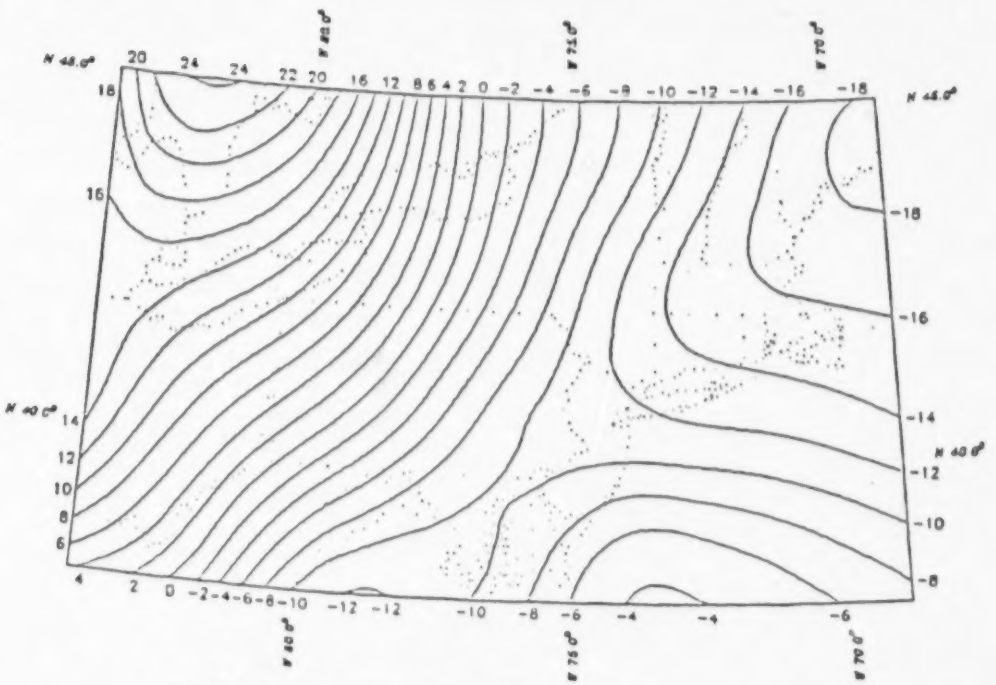

Preliminary Vorticity Field (10-6 sec-1)

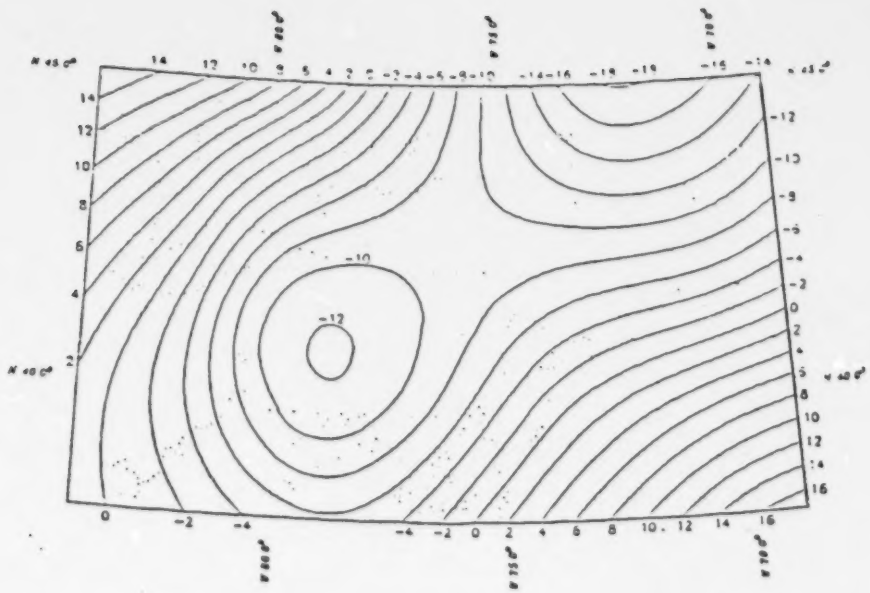

Barnes analysis of point values of divergence from the Endlich and Clark method (10^{-6} sec^{-1})

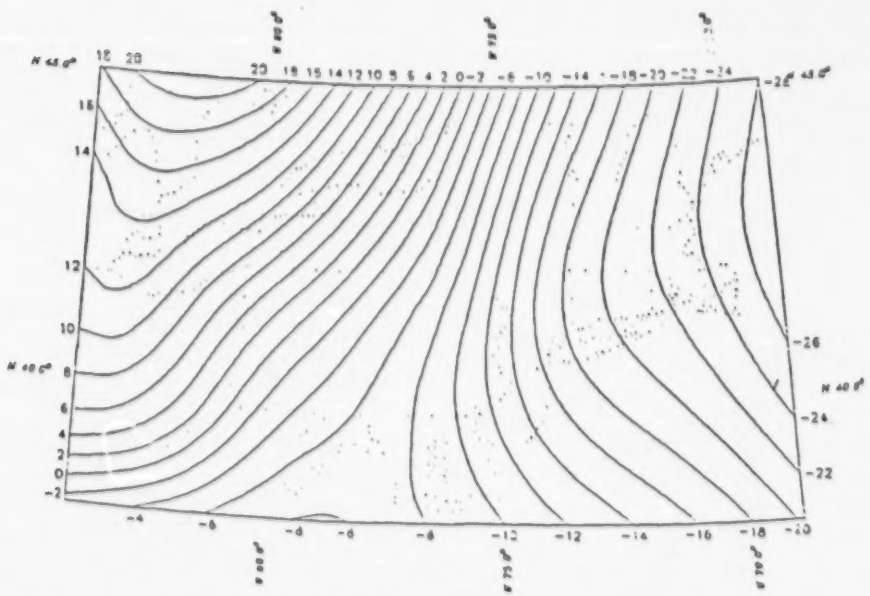

Barnes analysis of point values of vorticity from the Endlich and Clark method (10^{-6} sec^{-1})

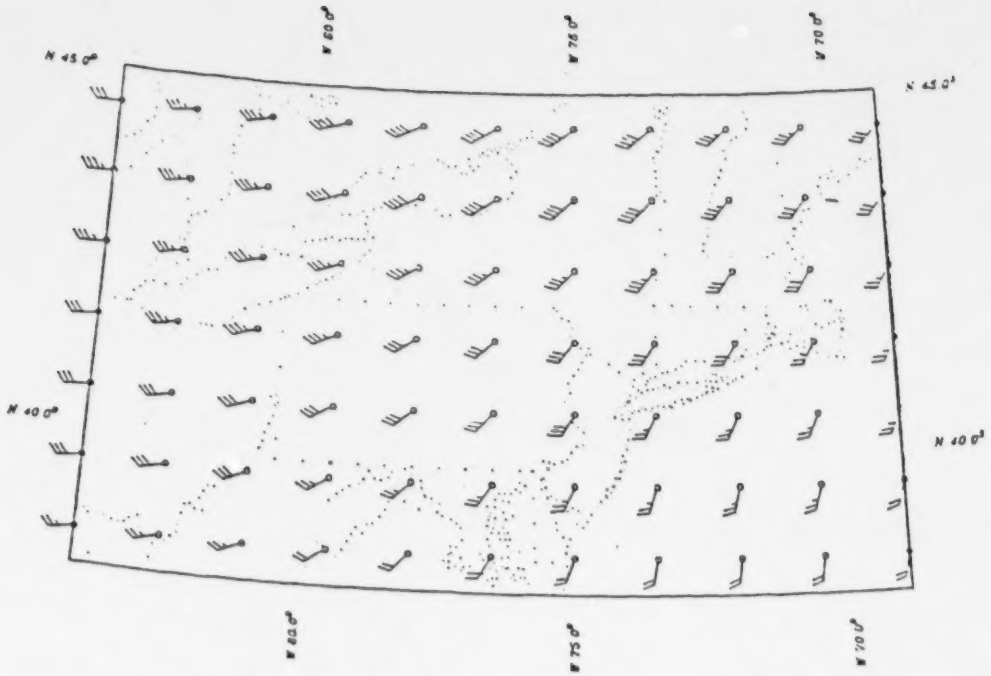

Final wind field from the Schaefer-Doswell method

STA.	LAT/LON	UST/VST		U/V		DIFF
72103	38.85 77.45	7.99	7.59	6.56	7.65	1.47
72425	38.37 82.55	13.43	3.63	11.93	3.44	1.51
72518	42.75 73.80	14.21	14.21	11.87	13.16	3.32
72529	43.50 80.22	15.97	5.81	13.28	6.26	2.73
72528	42.33 78.73	17.85	6.59	15.97	8.11	2.48
72606	43.65 70.32	10.61	12.64	10.33	12.40	.37
74456	43.65 73.78	5.66	12.14	5.87	12.03	.23
74494	41.67 69.97	6.55	12.04	6.75	11.55	.22

WIND FIELD VARIANCE = 3.66

WIND FIELD RMS = 1.91

WIND FIELD ADJ. ERROR = 1.54

Error Analysis

APPENDIX D - CALCULATION OF GRADIENTS FROM THE METHOD OF OVERLAPPING POLYNOMIALS

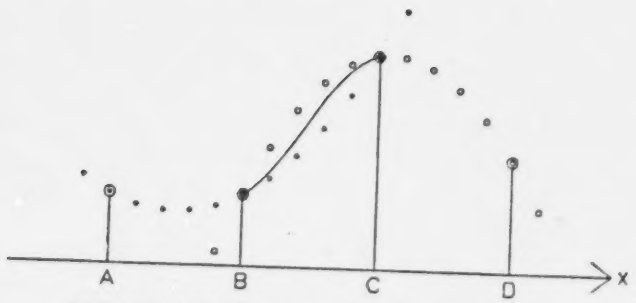

OVERLAPPING POLYNOMIAL FIT BETWEEN "B" AND "C"

When using the method of "overlapping polynomials" to interpolate between data points, a value estimate at any point between B and C is obtained from a linear weighting of the exact values of each parabola, ABC and BCD. Therefore an exact equation for the resulting interpolated line between B and C is,

$$y = \frac{(A_1x^2+B_1x+C_1)(X_C-x) + (A_2x^2+B_2x+C_2)(x-X_B)}{(X_C-X_B)}$$

which can be expanded to give,

$$y = \frac{(-A_1x^3+(A_1X_C-B_1)x^2+(B_1X_C-C_1)x+C_1X_C)+ (A_2x^3+(B_2-A_2X_B)x^2+(C_2-B_2X_B)x-C_2X_B)}{(X_C-X_B)}$$

By differentiating this equation and simplifying, the following equation results.

$$y' = \frac{3x^2(A_2-A_1) + 2x(B_2-B_1+A_1X_C-A_2X_B) + B_1X_C - B_2X_B + C_2 - C_1}{X_C - X_B}$$

For the calculation of gradients in this study, length was measured in terms of grid intervals such that $X_n - X_{n-1} = 1$. For every interpolation, the parabolic coefficients were determined using "A" as the location for the x origin, and thus $X_B = 1.0$ and $X_C = 2.0$. This results in the following simplified equation,

$$y' = 3x^2(A_2-A_1) + 2x(B_2-B_1+2A_1-A_2) + 2B_1 -B_2 + C_2 - C_1$$

which is evaluated for each output grid location between "B" and "C" to get gradients which are valid at the same locations as the interpolated values.

APPENDIX E - ERROR FIELDS ON 9 BY 5 TEST MATRIX USING THE SCHAEFER-DOSWELL PROCEDURE ON ACTUAL DATA

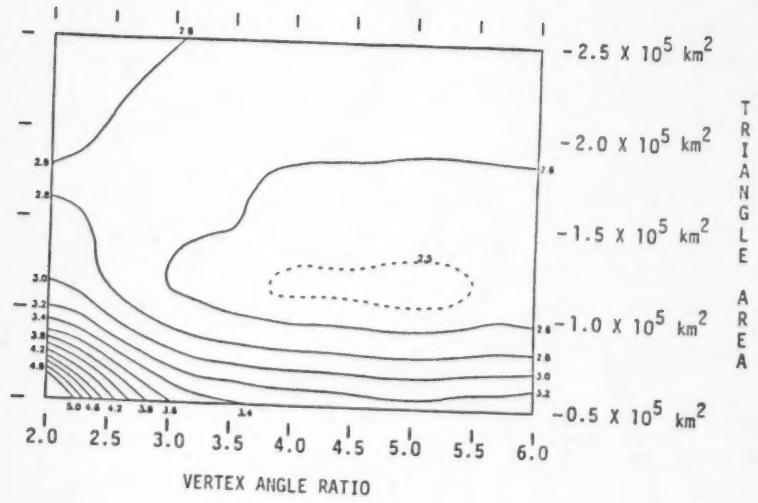

Root Mean Square (RMS) Error at Stations in m/s

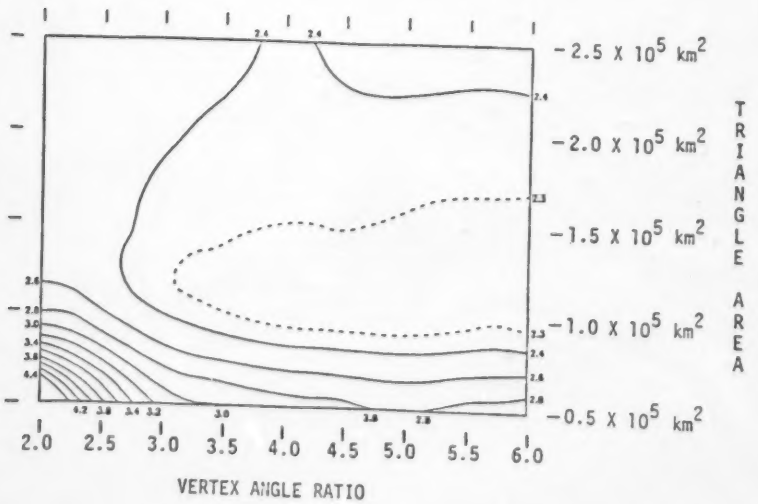

Average Absolute (AA) Error at Stations in m/s

APPENDIX F - ERROR FIELDS ON 9 BY 5 TEST MATRIX USING THE SCHAEFER-DOSWELL PROCEDURE ON ARTIFICIAL DATA WHEN A MODIFIED BARNES ROUTINE IS USED TO GRID MEASURED VALUES OF VORTICITY AND DIVERGENCE

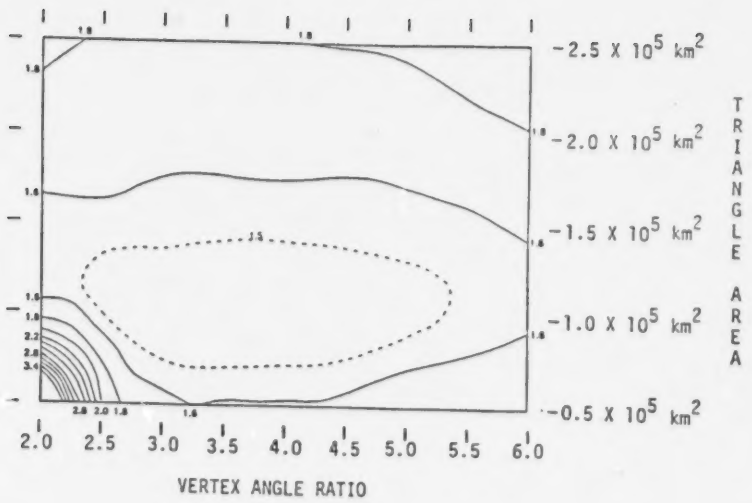

Root Mean Square (RMS) Error at Stations in m/s

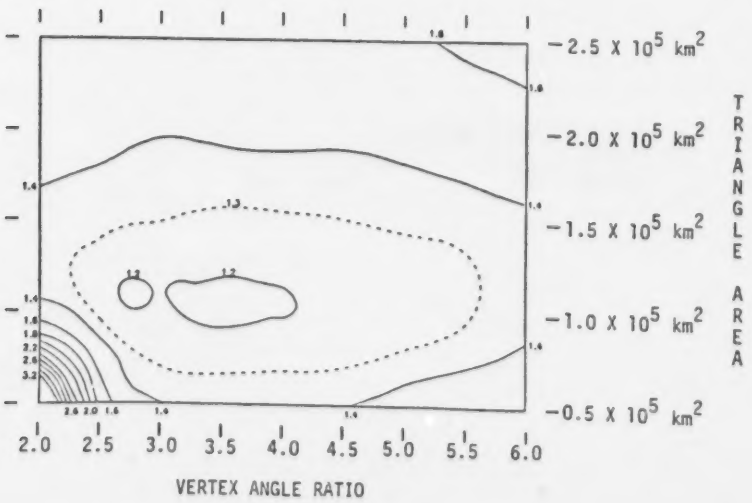

Average Absolute (AA) Error at Stations in m/s

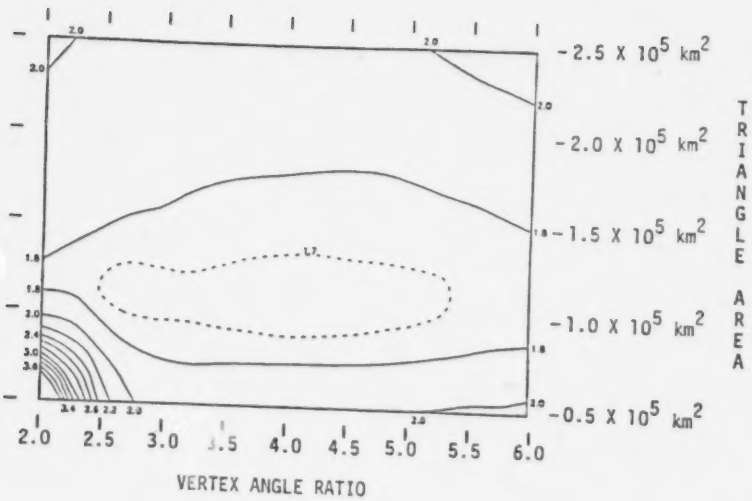

Root Mean Square (RMS) Error at Grid Points in m/s

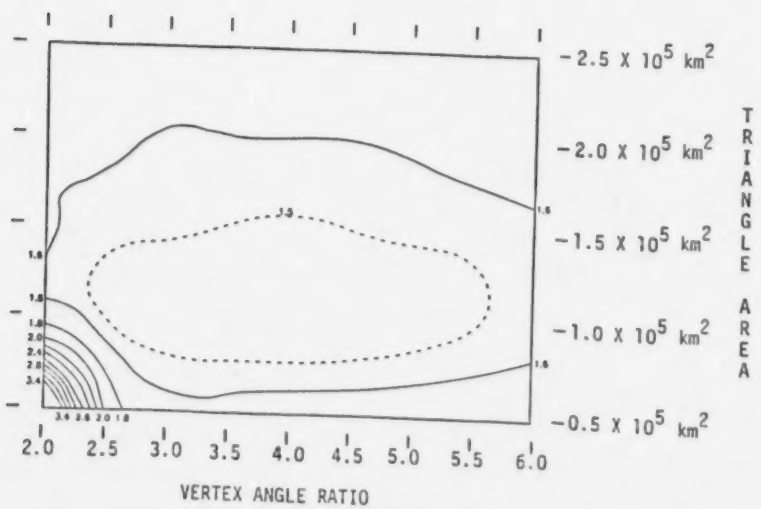

Average Absolute (AA) Error at Grid Points in m/s

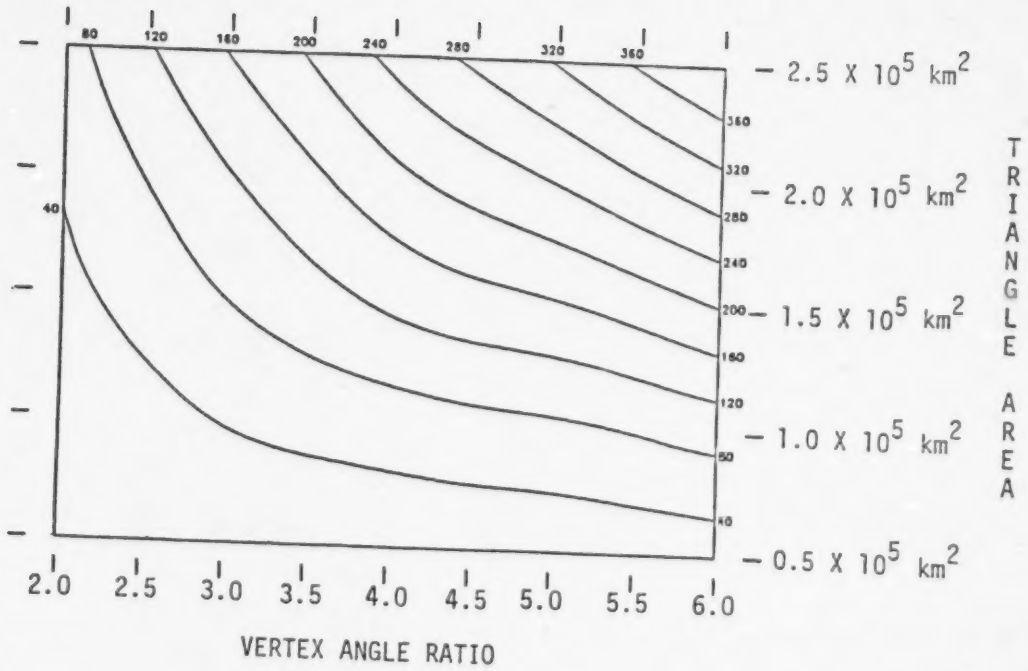

Number of Triangles Produced for the 9 by 5 Test Matrix

APPENDIX G - ERROR FIELDS ON 9 BY 5 TEST MATRIX USING THE SCHAEFER-DOSWELL PROCEDURE ON ARTIFICIAL DATA WHEN A PURE BARNES ROUTINE IS USED TO GRID MEASURED VALUES OF VORTICITY AND DIVERGENCE

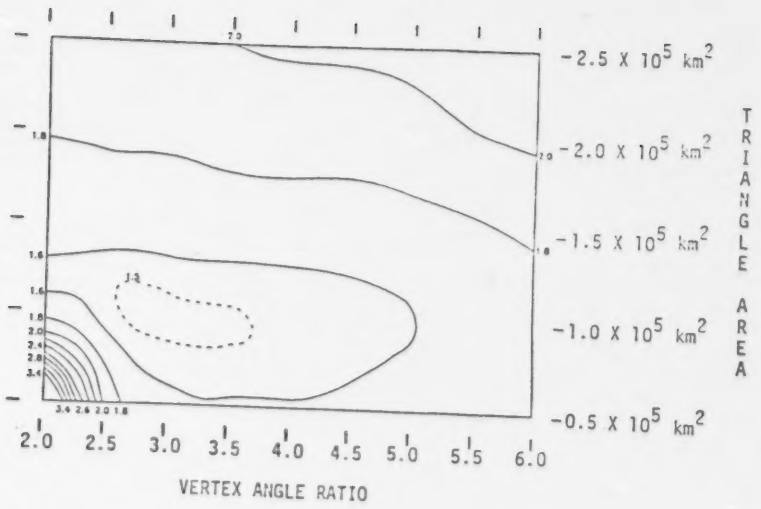

Root Mean Square (RMS) Error at Stations in m/s

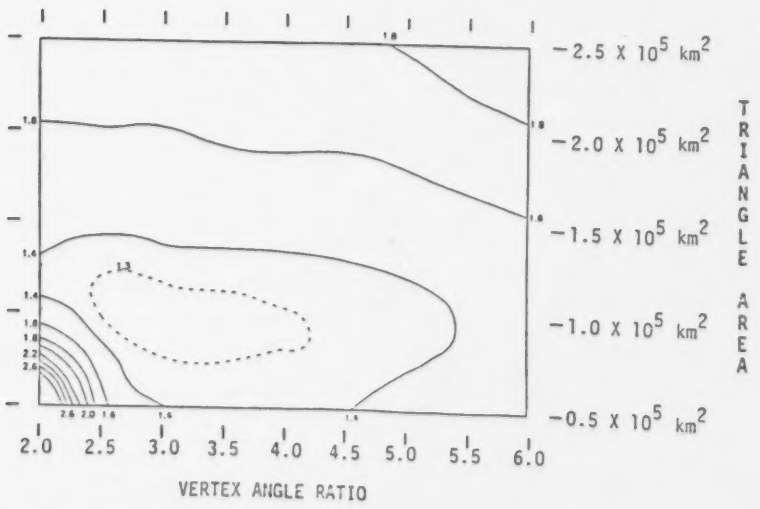

Average Absolute (AA) Error at Stations in m/s

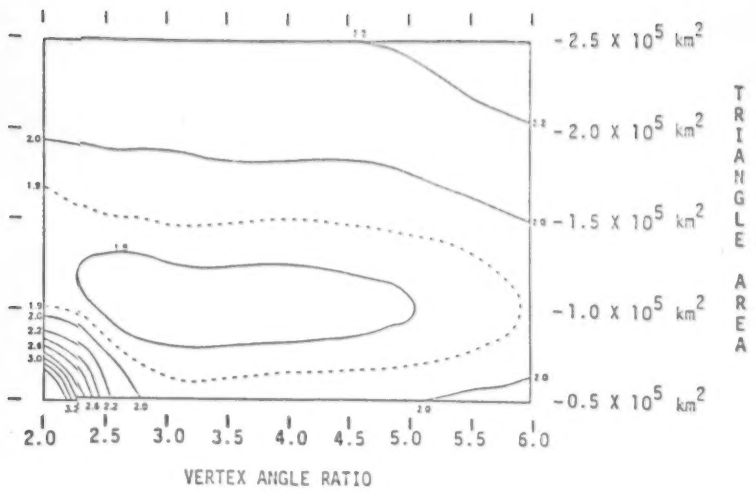

Root Mean Square (RMS) Error at Grid Points in m/s

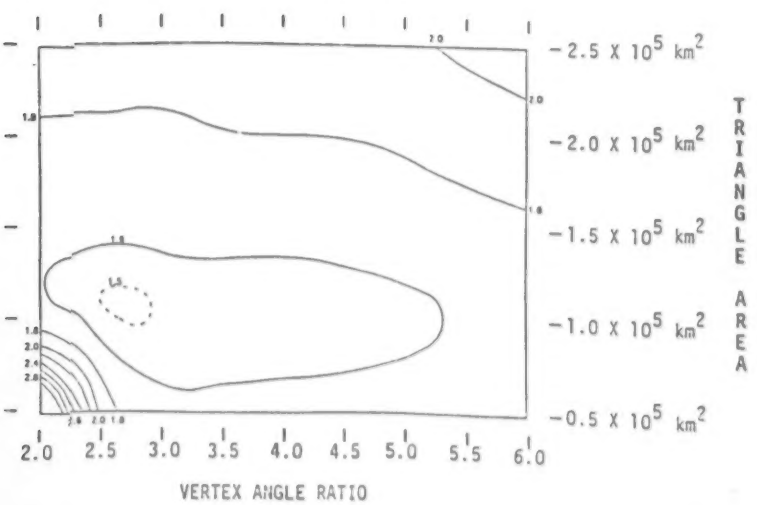

Average Absolute (AA) Error at Grid Points in m/s